https://doi.org/10.5194/bg-2019-189
Preprint. Discussion started: 20 June 2019

Biogeosciences Discussions

Successional patterns of (trace) metals and microorganisms in the Rainbow hydrothermal vent plume at the Mid-Atlantic Ridge

Sabine Haalboom[1,*], David M. Price[1,*,#], Furu Mienis[1], Judith D.L van Bleijswijk[1], Henko C. de Stigter[1], Harry J. Witte[1], Gert-Jan Reichart[1,2], Gerard C.A. Duineveld[1]

[1] NIOZ Royal Netherlands Institute for Sea Research, department of Ocean Systems, and Utrecht University, PO Box 59, 1790 AB Den Burg, Texel, The Netherlands

[2] Utrecht University, Faculty of Geosciences, 3584 CD Utrecht, The Netherlands

[*] These authors contributed equally to this work

[#] Current address: University of Southampton, Waterfront Campus, European Way, Southampton, UK, SO14 3ZH.

sabine.haalboom@nioz.nl; D.M.Price@soton.ac.uk

Keywords: Rainbow vent; Epsilonproteobacteria; Hydrothermal vent plume; Deep-sea mining; Rare earth elements; Seafloor massive sulfides

Abstract

Hydrothermal vent fields found at mid-ocean ridges emit hydrothermal fluids which disperse as neutrally buoyant plumes. From these fluids seafloor massive sulfides (SMS) deposits are formed which are being explored as possible new mining sites for (trace) metals and rare earth elements (REE). It has been suggested that during mining activities large amounts of suspended matter will appear in the water column due to excavation processes, and due to discharge of mining waste from the surface vessel. Understanding how natural hydrothermal plumes evolve as they spread away from their source and how they affect their surrounding environment may provide some analogies for the behaviour of the dilute distal part of chemically enriched mining plumes.

https://doi.org/10.5194/bg-2019-189
Preprint. Discussion started: 20 June 2019

This study on the extensive Rainbow hydrothermal plume, observed up to 25 km downstream from the vent site, enabled us to investigate how microbial communities change in the presence of a natural plume. The (trace) metal and REE content of suspended particulate matter (SPM) was determined using HR-ICP mass spectrometry and the microbial communities of the neutrally buoyant plume, above plume-, below plume-, and near-bottom water and sediment were characterised by using 16S rRNA amplicon sequencing methods. Both vertically in the water column and horizontally along the neutrally buoyant plume, geochemical and biological changes were evident as the neutrally buoyant plume stood out by its enrichments in (trace) metals and REEs, of which the concentrations changed as the plume aged. This was also reflected in the background pelagic system as Epsilonproteobacteria started to dominate and the biodiversity appeared to reduce with distance away from the Rainbow hydrothermal vent field. The Rainbow hydrothermal plume provides a geochemically enriched natural environment, which is a heterogeneous, dynamic habitat that is conducive to ecological changes in a short time span.

1 Introduction

Hydrothermal vent fields found at mid-ocean ridges and back-arc basins are known for discharging fluids rich in potential microbial energy sources such as H_2, H_2S, CH_4, NH_4 and Fe (Jannasch and Mottl, 1985; McCollom, 2000). In addition, they are characterised by the presence of polymetallic sulfide deposits containing high grades of metals like Cu, Co, Zn and rare earth elements (REE). Because of the steadily increasing demand for these metals, and their geo-political distribution on land, hydrothermal vent deposits are explored as new possible mining sites (Hoagland, 2010). Since such areas accommodate unique and vulnerable marine life, serious concerns exist about the environmental sustainability of seafloor massive sulfide (SMS) deposit mining (Boschen et al., 2013; Collins et al., 2013), especially with regards to the effects of plumes generated during the excavation of ores and by the return flow of wastes in the vicinity of hydrothermal vents (Ramirez-Llodra et al., 2011; Vare et al., 2018). As SMS mining will concentrate on deposits around hydrothermal vents, and not on active vents or chimneys due to technical risks associated with high temperatures (Gwyther et al., 2008), it is likely that the background and extinct vent communities (from microorganisms to megafauna) will be impacted through habitat loss,

https://doi.org/10.5194/bg-2019-189
Preprint. Discussion started: 20 June 2019

mechanical destruction, noise, smothering and bioaccumulation of toxic substances (Levin et al., 2016). However, knowledge about the background ecosystem and natural plume is sparse, as the vents and their proximal fauna have attracted most of the attention, for example in microbiology (e.g. Han et al., 2018; Cerqueira et al., 2018).

To fill this gap, the Dutch TREASURE project (STW-NWO) was focussed on describing the structure of the background pelagic and benthic communities of an active hydrothermal vent site with SMS deposits on the Mid-Atlantic Ridge (MAR). The Rainbow hydrothermal vent south of the Azores was selected for this study as it ejects one of the most prominent and persistent natural plumes on the MAR. Basic knowledge of natural plumes is essential to assess mining impacts for two reasons: firstly, hydrothermal plumes represent a distinct ecosystem in itself, which under the influence of currents may extend tens of kilometres away from its point of origin. The same currents will also disperse mining plumes, created in the vicinity of the hydrothermal vent. These mining plumes are therefore likely to interfere with the hydrothermal plume and thus potentially alter baseline (T0) conditions. Secondly, understanding natural plume processes may reveal how ecosystems adapt to elevated turbidity and co-occurring changes in the chemical environment.

Since the discovery of the Rainbow hydrothermal vent field in 1996 by German et al., several relationships concerning the composition of the hydrothermal fluid and the associated sediment formed by precipitation from the hydrothermal plume have been established. For example it was shown that the underlying host rock influences the hydrothermal fluid composition (Wetzel and Shock, 2000). Geochemical investigation of sediment by Cave et al. (2002) at distances of 2 to 25 km from the Rainbow hydrothermal vent field showed enrichments of Fe, Cu, Mn, V, As and P as a result of fallout from the hydrothermal plume. Studies of other hydrothermal vent systems demonstrated that deposition from the plume is partially being influenced by microbial activity which enhances scavenging and oxidation rates of metals (e.g. Cowen and Bruland, 1985; Cowen et al., 1990; Mandernack and Tebo, 1993; Dick et al., 2009), with implications for the local ocean geochemistry.

Microbial activity within the plume is fuelled by redox reactions that provide energy for chemotrophic microbial taxa. The abundance of energy sources within plumes support a plethora of chemotrophic

https://doi.org/10.5194/bg-2019-189
Preprint. Discussion started: 20 June 2019

microbial communities (e.g. Frank et al., 2013; Anantharaman et al., 2015). Plume microbial communities can be distinct or relatively similar to background communities (Dick and Tebo et al., 2010; Sheik et al., 2015; Olins et al., 2017), with plume associated bacteria originating from either seafloor communities, background seawater communities or from growth within the plume (Dick et al., 2013). Djurhuus et al. (2017) observed the dilution of vent associated microorganisms with increased redox potential, suggesting that communities associated with the rising plume would disperse with distance from the vent on a scale of metres, showcasing a variable community within the plume. After its initial rise, a hydrothermal vent plume becomes neutrally buoyant and is dispersed over potentially hundreds of kilometres (German and Sparks, 1993; Dymond and Roth, 1988), however this portion of the plume has not been sampled in a similar manner to identify microbial community patterns.

Overall, little is known about the chemical fractionation or microbial assemblages within the neutrally buoyant plume as it ages and disperses from the hydrothermal vent field. Notably, due to the lack of quantified characteristics of SMS mining plumes (especially the discharge plume), the T0 influence of this hydrothermal plume may act as an analogue for future mining plume impacts. Although it should be kept in mind that discharge plumes will have different physical characteristics as these plumes will have a higher initial density and therefore would tend to sink rather than maintain buoyancy and may have a different release depth. However, the natural plume could serve as an analogue for the finest and slowest sinking fraction of suspended solids in the mining plume. In this study, water column and sediment samples from the Rainbow hydrothermal vent area were investigated. Geochemical and biological changes were tracked vertically in the water column and horizontally along the neutrally buoyant plume, to study the heterogeneity in the background pelagic system that was influenced by the hydrothermal plume. By utilising a range of methods that could be useful as monitoring techniques and describing background environments that may be influenced by SMS mining, we contribute to site specific knowledge of the Rainbow hydrothermal vent plume behaviour, associated (trace) metal enrichments and microbial community composition.

https://doi.org/10.5194/bg-2019-189
Preprint. Discussion started: 20 June 2019

2 Material and methods

2.1 Study site

The Rainbow hydrothermal vent field (Fig. 1) is located on the Mid Atlantic Ridge (MAR) at 36°13.80 N, 33°54.14 W at approximately 2300 m water depth, southwest of the Azores. The vent field is located on the western flank on the non-volcanic Rainbow Ridge, in an offset between the South Alvin Mid Atlantic Ridge (AMAR) and AMAR segments of the MAR (Fouquet et al., 1998; Douville et al., 2002). It is located at the intersection between the non-transform fault system and the ridge faults (Charlou et al., 2002), making this vent field tectonically controlled. The vent field, which is approximately 100 by 250 m in size, is underlain by a basement composed of ultramafic rocks (Edmonds and German, 2004). The ultramafic setting of Rainbow is atypical for the region, which is dominated by basalt hosted vent systems (Douville et al., 2002). Due to serpentinization reactions during the circulation of the hydrothermal fluid in the peridotite basement rocks, the Rainbow vent field produced plumes particularly enriched in transition metals (notably Fe, Mn and Cu) and REE (Douville et al., 2002; Findlay et al., 2015). On the contrary the plumes are depleted in hydrogen sulfides (Charlou et al., 1997; Douville et al., 2002), resulting in relatively high metal/sulfide ratios. Consequently, the chimneys and the SMS deposits of the Rainbow hydrothermal field are enriched in Cu, Zn, Co and Ni when compared to vent systems with a basaltic host rock (Charlou et al., 1997).

The vent field consists of 10 active, high temperature (365 °C) black smokers and emits an extensive plume with a distinct chemical composition compared to the ambient seawater (Severmann et al., 2004). It is considered the largest and widest spreading plume in the region (German et al., 1996), rising up to 200 m above its source and was traced over 50 kilometres (Severmann et al., 2004). The plume dispersion is controlled by the local hydrodynamic regime and topography (Thurhnerr and Richards, 2001; Thurnherr et al., 2002), moving predominantly to the north and east around the Rainbow Ridge with an average current speed of 5-6 cms^{-1} and continues in a northward direction along the southern and eastern side of the rift valley of the AMAR segments (Edmonds and German, 2004). The plume characteristics and prior knowledge of its behaviour make the Rainbow vent field a suitable site to study neutrally buoyant plumes.

https://doi.org/10.5194/bg-2019-189
Preprint. Discussion started: 20 June 2019

2.2 Water column profiling and sampling

Water samples and sediment cores were collected along the gradient of the plume during RV *Pelagia* cruise 64PE398 in April 2015. Five putatively distinct biotopes were sampled: (i) above plume (1000 m water depth), (ii) plume, (iii) below plume (10 metres above bottom), (iv) near-bottom water and (v) sediment. Using CTD casts with a CTD-Rosette system, the plume was traced in real time using turbidity as an indicator, measured in NTU with a WETLabs turbidity sensor. Other variables measured included temperature (°C), salinity (PSU), density (σ-θ, kgm^{-3}), dissolved oxygen (mlL^{-1}) and chlorophyll (μgL^{-1}). At five stations, continuous yoyo CTD-casts were taken over the course of 12 hours, to study the temporal changes of the hydrothermal plume.

A total of 41 water samples were collected using 12 L Niskin bottles from eleven downstream stations, two distal downstream stations and three upstream stations. Once the CTD was back on deck, three distinct water samples were immediately taken for suspended particulate matter (SPM), trace metals, and the microbial community. Additional intermittent water samples were taken for nutrients and suspended particulate organic matter (Table 1).

Sediment and near-bottom water samples were collected with a NIOZ designed box corer of 50 cm diameter equipped with a top valve to prevent flushing, subsequently trapping more than 1.5 litres of near-bottom water (van Bleijswijk et al., 2015). In total eight cores were collected (Table 1). Due to unsuitable coring substrates, CTD locations and coring sites did not always follow the same track. Cores were taken on the eastern part of the Rainbow Ridge, continuing in the basin east of the ridge, while two cores were taken on the north-western flank of the ridge, following the path of the plume.

2.3 Suspended particulate matter analysis

From each 12 L Niskin bottle, two 5 L subsamples were collected to determine the concentration of SPM. The subsamples were filtered on board over pre-weighed 0.4 µm polycarbonate filters. The filters were rinsed with ~10 ml of Milli-Q water to remove salt, while still applying under pressure, and subsequently stored at -20 °C on board. Prior to analysis the filters were freeze dried. The samples were weighed in

https://doi.org/10.5194/bg-2019-189
Preprint. Discussion started: 20 June 2019

duplo, or once again if the difference between the two measurements was 0.03 mg or more. To yield SPM concentrations, the net dry weight of the SPM collected on the filters, corrected by the average weight change of all blank filters, was divided by the volume of filtered seawater. Subsequently, the filters were examined using a Hitachi TM3000 table-top SEM connected to an EDS-detector to visualize content of the SPM and analyse the chemical composition.

2.4 Chemical analysis

In order to examine the trace metals present in and around the hydrothermal plume, water samples were filtered over acid-cleaned 0.45 µm polysulfone filters directly from the Niskin bottle at ambient temperature while applying under pressure. A water barrel in between the filtration holder and pump allowed for volume measurements of water filtered. The filters were subsequently stored at -20 °C until further examination and were left to dry in an Interflow laminar flow bench at room temperature prior to analysis. The filters were placed in acid-cleaned Teflon vials and were subjected to a total digestion method. For this purpose a mixture of 6.5 ml HNO_3 (ultrapure)/HF (10:1) solution, 1 ml HCl and 1 ml $HClO_4$ was added to the vials, after which the vials were covered and placed in an Analab hotblock for 48 hours at 125 °C. After the filters were completely dissolved, the covers were taken off from the vials and the vials were left for 24 hours in order to evaporate the acids. Finally, the residue was taken up again in 10 ml HNO_3, pre-spiked with 5 ppb scandium and 5 ppb rhodium as internal standards. A HR-ICP-MS (Thermo Element II) was used to analyse the concentrations of major- and trace metals, as well as REEs.

2.5 Microbial community

Three distinct samples of 2 L of water were collected from three different Niskin bottles for Next Generation Sequencing (NGS). The water was filtered immediately after collection through a 0.2 µm polycarbonate filter (Nuclepore) facilitated by a vacuum of 0.2 bar at 4 °C, to limit DNA degradation. With a sterilised spatula, >0.25 grams of surface sediment were scraped off from the box cores whilst 1.5

https://doi.org/10.5194/bg-2019-189
Preprint. Discussion started: 20 June 2019

184 litre of overlying (near-bottom) water was filtered as above. Filters were stored in a 2 ml cryo-vial and all
185 samples were stored at -80 °C on board.

186 DNA was extracted using a Power Soil DNA Isolation Kit (MoBio, now Qiagen) according to the
187 manufacturer's protocol. Each DNA extract concentration was quantified using a Qubit 3.0 fluorimeter
188 (Qiagen, Inc.) and stored at -20 °C before amplification. Extracts were combined with Phusion Taq
189 (Thermo Scientific), High Fidelity Phusion polymerase buffer and universal primers to amplify the V4
190 region of 16 S rDNA of bacteria and archaea (Table 2), with unique molecular identifier (MID)
191 combinations to identify the different samples. All negative controls from all PCR series were labelled
192 with the same unique MID. The PCR settings were as follows: 30s at 98 °C, 29 cycles (10s at 98 °C, 20s
193 at 53 °C, 30s at 72 °C) and 7 minutes at 72 °C. Four and three samples were re-run at 30 and 32 cycles,
194 respectively, in order to yield enough product. Each sample was subjected to the polymerase chain
195 reaction (PCR) protocol in triplicate and processed independently to avoid bias. 5 µl of product was used
196 to screen the products on an agarose gel. The remaining 25 µl of each triplicate was pooled to evenly
197 distribute the DNA, split into two slots and run on a 2 % agarose gel at 75 volts for 50 minutes. Sybergold
198 stain was applied post run for 20-30 minutes before cutting the 380 bp bands out with a sterilised scalpel
199 over a blue light to avoid UV damage. The two bands of mixed triplicates were pooled, purified using the
200 Qiaquick Gel Extraction Kit (Qiagen, Inc.) and quantified with a Qubit™ 3.0 fluorometer (Qiagen, Inc.).
201 Samples were pooled in equimolar quantities together with blank PCR controls. The pooled sample was
202 concentrated using MinElute™ PCR Purification columns (Qiagen Inc.) as described by the manufacturer
203 and sent to Macrogen (South Korea) for sequencing. Sequencing was undertaken with a Roches GS FLX
204 instrument using Titanium chemistry on a one-eight region gasket and Roche GS FLX instruments.
205 Sequence processing was undertaken as described by van Bleijswijk et al. (2015), using a QIIME pipeline.
206 Sequences shorter than 250 bases and average Q scores below 25 were removed. The OTU sequences
207 (>98 % similarity) were classified (>93 % similarity) based on a recent SILVA SSU database (release
208 132; Yilmaz et al. 2014). Single reads were excluded and all data were standardised to remove any
209 disproportionate sampling bias.

210

https://doi.org/10.5194/bg-2019-189
Preprint. Discussion started: 20 June 2019

211 ## 2.6 Statistics

212 Unconstrained ordination techniques were utilised to distinguish biotopes and general community
213 patterns. Non-metric Multi-Dimensional Scaling plots (NMDS) were created based upon Bray-Curtis
214 similarity matrices of square root transformed microbial community assemblages. Group average
215 clustering was also utilised in order to quantify similarities between the samples. ANalysis Of SIMilarities
216 (ANOSIM) was subsequently used to statistically test community distinctions based upon presumed
217 biotopes (sediment, near-bottom water, below plume water, plume water and above plume water). In
218 addition, all water column samples were plotted in separate NMDS plots to observed patterns in greater
219 detail. Physical properties of all water samples (station, depth, turbidity and location) were depicted in a
220 NMDS plot to observe sample similarities. These environmental data were normalised and Euclidean
221 distance was used to create a similarity matrix. The relationship between Fe and turbidity was tested with
222 a linear regression analysis. Trace metals and REE were normalised to Fe, since it is the primary particle-
223 forming element at all stages of plume dispersion, giving insight in the chemical behaviour. All
224 multivariate statistics were undertaken in Primer™ V6 (Clarke and Gorley, 2006).

225 Shannon-Wiener index (log e) was calculated as a diversity measure. Biodiversity differences between
226 biotopes were tested with the non-parametric test Kruskal-Wallis with pairwise comparisons as the data
227 did not meet normality or homogeneity assumptions, even after transformation. These statistical tests
228 were undertaken in SPSS.

229 A SIMililarities PERcentage analysis (SIMPER in Primer v6) was applied on the microbial class level
230 with a cut off for low contributions at 90 % based on Bray-Curtis similarity matrix to characterise the
231 community composition based on groups contributing to intra biotope similarities. Relationships between
232 environmental variables and microbial classes as a percentage of each composition within the plume,
233 were tested with Pearson correlation and hierarchical clustering to identify broad response groups.

234

235

236

https://doi.org/10.5194/bg-2019-189
Preprint. Discussion started: 20 June 2019

3 Results

3.1 Water column characteristics

Temperature, salinity and density plots indicated that the water column at each location had similar physical traits, whereby three different water masses could be distinguished (Supplement Fig. S1). The surface Eastern North Atlantic Central Water (ENACW) was characterised by a temperature, salinity and density at the surface of 18 °C, 36.4 PSU and 26.2 kgm^{-3} to 11 °C, 35.5 PSU and 27.2 kgm^{-3} at the bottom of the water mass. The underlying Mediterranean Outflow Water (MOW) was characterised by a temperature of 7.5-11 °C, a salinity of 35.4-35.5 PSU and a density of 27.2-27.75 kgm^{-3}. The North Atlantic Deep Water (NADW) was characterised by temperatures ranging from 4 to 7.5 °C, salinity of 35.0 to 35.4 PSU and a density of 27.75 to 27.825 kgm^{-3} (Emery and Meincke, 1986). The neutrally buoyant plume was centred around the 27.82 kgm^{-3} isopycnal, as illustrated in Figures 2 and 3.

3.2 Turbidity and plume dispersion

Against a background of non-plume influenced waters with typical concentrations of SPM of 0.04 mgL^{-1} (0.015 NTU), the neutrally buoyant plume stands out as a layer of distinctly higher turbidity values (i.e. higher SPM concentrations) in the depth interval of 1750 – 2400 m (Fig. 2). The apparent continuity of this turbid water layer, especially to the NE of the Rainbow field, and lack of similarly turbid waters in the bottom waters below the plume, link the plume to Rainbow and preclude an origin in local sediment resuspension.

At downstream stations, a consistent trend of decreasing turbidity and increasing vertical dispersion was noted. At station 27, 3.5 km north of Rainbow, maximum turbidity in the core of the plume was 0.15 NTU (0.09 mgL^{-1}) and plume thickness was about 105 m, whilst at station 46, 15.2 km east of Rainbow, maximum turbidity was only 0.08 NTU (0.06 mgL^{-1}) and plume thickness was 275 m. Away from the main plume path, station 47 and 49 (13.8 and 16.5 km from Rainbow, respectively) showed a diluted signature similar to that observed at the most distal stations along the main plume path. Despite being most proximal to Rainbow, station 16, located 1.0 km downstream of Rainbow, showed a relative low

https://doi.org/10.5194/bg-2019-189
Preprint. Discussion started: 20 June 2019

turbidity of 0.015 NTU (0.04 mgL^{-1}). Since the plume is more constrained closer to the source, the main body of the narrower plume could have been missed with the CTD. Stations upstream of the vent site (station 13 and 28, 4.2 and 7.5 km southwest of Rainbow respectively and station 40, 3.6 southeast of Rainbow) displayed low turbidity values, ranging between 0.01 and 0.02 NTU (0.04 mgL^{-1}) (Fig. S2).

The CTD profiles from stations 42 and 49 (4.9 and 16.5 km north of Rainbow respectively) both displayed highest turbidity in the lower hundreds of metres above the seafloor, with instances of seafloor contact during time of sampling. Therefore no samples could be taken below the plume at these stations. The assumption that the plume is subject to vertical movement is supported by observations made during 12-hour CTD yoyo casts carried out at station 27 (Fig. 3). Along with vertical displacements of the 27.82 kgm^{-3} isopycnal on the order of 150 m, likely reflecting internal tidal motions, the hydrothermal plume was found to also move up and down, at times touching the seafloor.

3.3 Enrichment of (trace) metals compared to the ambient seawater

NMDS ordination (Fig. 4) based on Euclidean distance resemblance of normalised element/Fe molar ratio data of all collected water samples (2D stress = 0.03), revealed a clear distinction of the different samples. Most outstanding are the samples from above plume waters, indicating that the chemical composition is different from the other samples.

The remaining samples showed less variation, nonetheless the samples collected from below the plume and the samples collected away from the main path of the plume can be distinguished. This shows that the hydrothermal plume can be characterised by its chemical composition. When comparing samples taken in the turbidity maximum of the plume to the above plume water samples taken at 1000 m water depth it is found that Fe, Cu, P, V and Pb are enriched by factors of ~80, ~90, ~17, ~52 and ~25 respectively. Elements with a more moderate degree of enrichment are Co, Mn, Zn, Al and Ni, with enrichment factors of ~8.0, ~2.5, ~10.3, ~1.4 and ~1.6, respectively. The REEs were enriched by a factor of 5 to 40 relative to the clear water. U, Ti and Ca are slightly enriched at turbidity maxima, by factors of ~1.3, ~1.6 and ~1.2, respectively. In and Sn are depleted compared to the clear water above the plume.

https://doi.org/10.5194/bg-2019-189
Preprint. Discussion started: 20 June 2019

3.4 Geochemical gradients within the hydrothermal plume

Within the hydrothermal plume, geochemical evolution is found as the plume disperses. Visual examination of the samples with the SEM coupled with chemical analysis performed with the EDS-detector revealed that the SPM within the plume close to the Rainbow hydrothermal vent at station 32 (2.9 km north of Rainbow) mainly consisted of Fe-sulfides. In the plume samples further downstream, Fe is mainly present as Fe-oxides, Fe-hydroxides or bound in alumino-silicates.

Chemical examination of the samples showed gradients in the element/Fe molar ratios along the path of the plume as well as off the main path of the plume at upstream and the most distal downstream stations. Since the Fe concentration is linearly related to the turbidity (Fig. 5) (R^2 = 0.9356), normalisation to Fe reveals relative enrichments or depletion of common elements. The chalcophile elements Co, Cu and Zn show a partly-linear relation steepening with increasing Fe concentration (Fig. 6A), indicating that the element/Fe molar ratios are elevated close to the source but decrease towards the more distal sites (Fig. 7A). One exception is the Zn/Fe molar ratio, which is elevated at station 37, 39 and 44. The oxyanions P and V are linearly related to Fe (Fig. 6B), therefore they also display more or less constant molar ratios, both upstream and downstream of Rainbow (Fig. 7B). The REE show a partly-linear relation levelling-off with increasing iron concentrations (Fig. 6C). Within the plume this is displayed as increasing element/Fe molar ratios towards station 44, with station 42 as an exception, followed by a constant or slightly decreasing molar ratio from station 44 onwards (Fig. 7C). The Ca/Fe molar ratios ranged between 0 and 15 for most of the downstream stations, apart from the stations further downstream (47 and 49), which displayed slightly higher Ca/Fe molar ratios. Upstream station 28 had a Ca/Fe molar ratio similar to those found at station 47 and 49 and upstream station 40 was found to have a significantly higher Ca/Fe molar ratio. Other analysed elements, Mn, Al, Ni, In, Pb, Ti and U showed no clear relationship with the Fe concentration (Fig. 6D). However, within the plume it was found that the Mn/Fe molar ratio is lower than at the upstream stations or the more distal downstream stations.

https://doi.org/10.5194/bg-2019-189
Preprint. Discussion started: 20 June 2019

315 ### 3.5 Microbial assemblages in water column biotopes

316 Samples from sediment, near-bottom water and above plume water contained microbial communities
317 which clustered distinctly from each other and from plume and below-plume communities (Fig. 8). In
318 particular, sediment and near-bottom water samples have communities that are very dissimilar from the
319 overlying water column samples. Sediment samples appeared to cluster in a straight line suggesting some
320 sort of gradient of similarity along the ordination axis, though no apparent patterns were observed when
321 independently plotted. The near-bottom water samples were relatively dispersed in the MDS plot
322 suggesting a more variable community. Samples taken at the upstream station 13 from below-plume and
323 plume depths showed no similarity with analogous samples from the other stations, except for the above
324 plume community which is consistent with other stations. In general, plume and below-plume
325 communities were more similar nearer to the vent source, with stations further downstream displaying
326 greater dissimilarity (Fig. 9, Fig. S3).

327 Group average cluster analysis showed high level of dissimilarity, i.e. large community variation, between
328 and within biotopes. ANOSIM revealed all putative biotopes that were sampled had distinct communities
329 (Global R = 0.738; p = 0.001; 999 permutations), except for plume and below plume samples which could
330 not be distinguished statistically (Global R = -0.091; P = 0.861). The two seemingly unique samples from
331 station 13 also tested significantly distinct, but with a low number of permutations (<999) due to low
332 replication (n=2).

333

334 ### 3.6 Univariate biodiversity

335 Plume and below plume samples were less diverse than sediment samples, whilst diversity in the plume
336 was lower than in near-bottom water samples (Kruskal-Wallis: $\chi 2$ (4) = 36.127, P <0.01). In general,
337 plume diversity was low (Fig. 10), but further differences were not statistically significant, likely due to
338 limited replication and intra biotope variation.

339 The plume microbial community at sites upstream of Rainbow and at the immediate downstream sites
340 (stations 28, 16 and 27) showed similar and relatively high biodiversity (>4.5) (Fig 11). Plume

https://doi.org/10.5194/bg-2019-189
Preprint. Discussion started: 20 June 2019

biodiversity at the sites further away from Rainbow gradually decreased until station 46, which displayed the lowest Shannon index value of 2.4. Distant stations 47 and 49, showed biodiversity rising to a more moderate index value around 3.5.

3.7 Species composition

Results of the SIMPER analyses showing the contributions of taxa composition to similarities within biotopes (Table 3), mirrored the NMDS and ANOSIM results whereby the similarity of community composition in each biotope was dominated by a different makeup of the microbial community. The Archaeal class Nitrososphaeria (Marine group 1 archaea) contributed the most to similarity within the above and below plume water communities, while also being very common in all water samples. Alphaproteobacteria, Gammaproteobacteria and Deltaproteobacteria also constituted as a large makeup of all biotopes in the area. The class Epsilonproteobacteria were largely absent from above plume samples being not influenced by the plume, and only contributed <2 % to near-bottom water communities. By contrast, Epsilonproteobacteria were dominant in plume water samples (accounting for >35 % of the community), and were the fifth most dominant taxon in below plume water samples contributing 8.9 % of the community.

Epsilonproteobacteria accounted for about 20 % of the plume community at stations near the vent. Beyond the near vent stations, an increase in relative abundance of Epsilonproteobacteria with distance from vent was observed, accounting for 64 % of the community at the distant station 46 (Fig. 12). Alphaproteobacteria, Deltaproteobacteria and Gammaproteobacteria appeared to become less dominant with distance from the plume source (Fig. 12). The communities at distant stations 47 and 49 were less dominated by Epsilonproteobacteria (around 40 %). Below plume communities were dominated mostly by Nitrososphaeria (Marine group 1 Archaea) whereby Nitrosphaeria became more dominant with distance from the plume source likewise as the Epsilonproteobacteria in the plume. Correlations between environmental variables (elemental chemistry and physical properties) and all microbial classes observed in the plume were evident and appeared class specific (Fig. S4). The hierarchical clustering revealed eight broad response groups, which displayed different relationships with the environmental variables.

https://doi.org/10.5194/bg-2019-189
Preprint. Discussion started: 20 June 2019

368 # 4 Discussion

369 Using a multidisciplinary approach in which physical, geochemical and ecological data were collected
370 from the Rainbow vent neutrally buoyant plume and its underlying sediment, we aimed to expand
371 knowledge of the T0 state of the background ecosystem of a hydrothermal vent. Such knowledge is
372 deemed essential to be able to assess (potential) impacts of future deep-sea SMS mining. We found
373 differences between the plume and background water composition with identified distinct biotopes. In
374 addition, pertinent chemical and biological gradients within the extensive Rainbow hydrothermal vent
375 plume were evident.

376

377 ## 4.1 Physical constraints of plume location and behaviour

378 The plume was observed within the NADW mass, constrained to an isopycnal density envelope of 27.82
379 kgm^{-3} (Fig. 2 and 3). Using turbidity measurements and presumed plume path, we traced the plume up to
380 25 km away from the vent source, in agreement with observations made by German et al. (1998) of a
381 plume greater than 50 km, that is controlled by local hydrodynamics and topography. Unexpectedly, in
382 the basin upstream of the Rainbow vent field a turbidity peak at 1975 m water depth resembling a plume
383 was observed as well, confounding our assumption of a clear water column at upstream stations and
384 distant downstream stations. This indicates that the plume is reaching further than previously observed
385 by Thurnherr and Richards (2001) and German et al. (1998). This is exemplified by the local variation in
386 microbial community composition of upstream stations (Fig. 12) and is supported by the relatively low
387 Ca/Fe molar ratio at station 28 (Fig. 7), indicating hydrothermal influence. In addition, the observed
388 variability of plume strength and vertical position (Fig. 3) indicate that local fluctuation in the current
389 regime and tidal motions influence the plumes behaviour. This dynamic behaviour has implications for
390 surveys designs and should be considered when monitoring natural and man-made plumes, such as
391 mining-related plumes. Prior insight into plume extension and behaviour is required for the identification
392 of adequate control sites and for tracking of plume evolution in future impact studies.

393

https://doi.org/10.5194/bg-2019-189
Preprint. Discussion started: 20 June 2019

4.2 Plumes influence on the water column chemical and microbial make-up

The neutrally buoyant plume introduced pelagic heterogeneity in terms of chemical and microbial composition, which is supported by the vertical classification of the different biotopes. The neutrally buoyant plume was evidently enriched in metals and REE compared to overlying clear water. Element concentrations were found to be in line with those found by German et al. (1991) and Edmonds and German (2004) who have studied the Trans-Atlantic Geotraverse (TAG) hydrothermal plume and the Rainbow hydrothermal plume, respectively. Our chemical results from Rainbow also match with those of Ludford et al. (1965), who have studied vent fluid samples from the TAG, Mid-Atlantic Ridge at Kane (MARK), Lucky Strike and Broken Spur vent sites, i.e. element concentrations were found to be in the same order of magnitude.

The distinctive chemical composition of the plume samples (e.g. metal concentrations) affects chemotrophic microbial growth within the plume as indicated by the typical microbial community in plume samples. Unlike Sheik et al. (2015), we observed a clear and consistent separation between communities in the plume and those in above-plume samples. The influence of MOW on the above-plume community could also play a role, as oceanic water masses can harbour different microbial communities (Agogue et al., 2011). However, the palpable presence of a plume in the turbidity data with supporting chemical measurements, and the occurrence of vent associated Epsilonproteobacteria (Olins et al., 2017; Djurhuus et al., 2017) and other vent associated groups such as SUP05 (Sunamura et al., 2004), point to a unique chemical environment. Here chemosynthetic communities flourish and give rise to independent biotopes in the neutrally buoyant plume kilometres downstream of the vent site.

Below-plume communities were not distinct from the plume biotope, although instead of Epsilonproteobacteria, the ubiquitous class Nitrososphaeria was the most dominant group, reflecting some similarities with above-plume seawater communities. Similarities between plume and proximal habitat communities has also been observed by Olins et al. (2017), whereby intra-field (defined as within vent field between diffuse flows) and diffuse flow microbial communities were alike. In our study, similarities between plume and below-plume are likely derived by precipitation of mineral and microbial aggregates dragging plume microbes deeper below the plume as suggested by Dick et al. (2013). In

https://doi.org/10.5194/bg-2019-189
Preprint. Discussion started: 20 June 2019

addition, internal wave induced turbulence causes vertical mixing along the slope of the Rainbow Ridge (van Haren et al., 2017), which may cause the plume and associated communities near the vent field to mix with ambient water communities leading to assemblage similarities. This indicates the plume and associated microbial processes could have a larger vertical footprint than previously observed, supporting suggestions by Olins et al., (2017) that proximal non-plume habitats have been overlooked. Interestingly, near-bottom water (and sediment) community assemblages were distinct from the below-plume and other water column communities. This could imply: 1) that there is little ”fall out” from the plume at distance from the vent which is in agreement with sediment trap observations by Khripounoff et al. (2001), 2) plume specific bacteria die off due to lack of energy sources and DNA degrades before reaching the seafloor, 3) microbes are more abundant in the near-bottom waters, either naturally or through mechanical disturbance resuspending sediment during the coring process, outnumbering groups that have been mixed in from overlaying water. Despite the presence of a plume and precipitation, a barrier between the sea floor and the water column biotopes is present, consistent with global broad scale non-vent benthic-pelagic patterns (Zinger et al., 2011). According to Khripounoff et al. (2001) the fall-out from the Rainbow plume is spatially limited, as the extended chemical imprint on the sediment (reported by Cave et al. (2002), Chavagnac et al. (2005), and this study), is likely to have formed when the plume is in direct contact with the sediment during its vertical tidal migration. As the plume rises again, the associated distinct communities apparently resume dominance in the near-bottom water. Though Epsilonproteobacteria have been detected in Rainbow vent sediments comprising over 5 % of the sediment community (Lopez-Garcia et al., 2003), very few reads of this group in sediment samples were present in our study. Cave et al. (2002), observed chemical evolution of sediment composition with distance from source, thus we infer the dependence of sediment dwelling Epsilonproteobacteria on nearby plume precipitates, such as Cu, Zn and Cd. Additionally, DNA degradation rate can be 7 to 100 times higher in sediment than in the water column (Dell’Anno and Corinaldesi, 2004). Therefore, although our results suggest no microbial plume community imprint on the sediment, we cannot rule out short lived episodic community changes when the plume is in contact with the sediment.

https://doi.org/10.5194/bg-2019-189
Preprint. Discussion started: 20 June 2019

448 ### 4.3 Geochemical gradients within the hydrothermal plume

449 Analysis of SPM in water samples taken along the flow path of the plume, as well as off the flow path,
450 showed conspicuous trends of elements, reflecting the chemical evolution of the plume as it drifts away
451 from its hydrothermal source.

452 The chalcophile elements (Cu, Co and Zn) were found to have the highest element/Fe molar ratios closest
453 to the vent site, indicating either rapid removal from the hydrothermal plume or removal from the solid
454 phase as the plume drifts away from the vent site. Using SEM-EDS, it was demonstrated that at the
455 proximal downstream stations mainly Fe-sulfides were found, whereas Fe-(oxyhydr)oxides were found
456 further downstream. This suggests that chalcophile elements are mainly present in the form of sulfide
457 mineral particles at the proximal stations, which are entrained in the flow of hydrothermal water
458 emanating from the Rainbow vents and subsequently rapidly lost by settling from the plume in sulfide-
459 bearing phases, while a large portion of Fe remains is suspension (Cave et al., 2002; Edmonds and
460 German, 2004), consistent with decreasing concentrations of Cu, Zn and Cr in sediment recovered from
461 the Rainbow area with increasing distance to the vent site (Cave et al., 2002).

462 The oxyanions (V and P) showed constant element/Fe molar ratios with increasing distance away from
463 Rainbow, suggesting co-precipitation with Fe as oxyhydroxides (Edmonds and German, 2004). No
464 additional uptake of these elements was observed with increasing distance from the vent field (German
465 et al., 1991), since these elements are scavenged initially in significant amounts during the buoyant plume
466 phase (Cave et al., 2002).

467 The trend shown by Mn/Fe molar ratios can be attributed to the slower oxidation kinetics of Mn (Cave et
468 al., 2002). It takes longer for reduced Mn to be oxidised than it would for Fe, resulting in an increase in
469 particulate Mn with increasing distance from the Rainbow hydrothermal vent field, which subsequently
470 settles out from the plume as Mn-oxyhydroxides (Cave et al., 2002).

471 The observed positive relationship between the REEs and Fe is indicative of continuous scavenging of
472 these elements from the ambient seawater onto Fe-oxyhydroxides (Caetano et al., 2013; Edmonds and

https://doi.org/10.5194/bg-2019-189
Preprint. Discussion started: 20 June 2019

German, 2004). Therefore, the highest element/Fe molar ratios were observed away from the Rainbow hydrothermal vent site, where Fe-(oxyhydr)oxides are dominant more distal to the vent site.

The Ca/Fe molar ratios vary between 0 and 14 for the stations downstream of the Rainbow hydrothermal vent, but are higher at the distant downstream station 47 and 49 and upstream stations 28 and 40. Especially at station 40, located on the Rainbow Ridge, the Ca/Fe molar ratio is significantly higher than at the other stations. This is in line with observations by Khripounoff et al. (2001) and Cave et al. (2002) who also found that the relative Ca concentration in settling particles and the sediments is lower close the Rainbow vent field and increases as the Fe concentration decreases when the plume disperses. Since Ca is naturally present in high abundances in pelagic skeletal carbonate which rains down from the overlying water column and Fe is mainly present as a hydrothermal component the Ca/Fe molar ratio could be an indicator for the extent of the hydrothermal influence. The high molar ratio at station 40 would then suggest that this station is hardly or not at all influenced by the hydrothermal plume, whereas station 28, 47 and 49 are, as expected, influenced in more moderate degrees compared with the stations directly downstream of Rainbow.

4.4 Microbial gradients within the hydrothermal plume

The microbial plume community composition and diversity altered with distance from the plume source showcasing a horizontal heterogeneity within the plume. Despite dilution, the vent associated group Epsilonproteobacteria (specifically the most common genus *Sulfurimonas*), appeared to dominate the community composition. This is likely due to its flexibility to exploit many sulfur compounds as electron donors, and oxygen and nitrate as acceptors (Nakagawa et al., 2005), making them suitable inhabitants of dynamic environments (Huber et al., 2003). It is unclear from the relative abundance data obtained, whether Epsilonproteobacteria dominate by rapid reproduction or if other groups decline in abundance. However, it is evident that Epsilonproteobacteria remain competitive or outcompete other competitors such as generalists Gammaproteobacteria that are often vent associated (i.e. SUP05). It is unlikely that this pattern is caused by entrainment of Epsilonproteobacteria from background seawater over time. This is based on the lack of significant presence of Epsilonproteobacteria in above-plume water and at remote

https://doi.org/10.5194/bg-2019-189
Preprint. Discussion started: 20 June 2019

station 13, and reduced mixing that neutrally buoyant plumes generally experience (McCollom, 2000). This is further supported by the increasing uniqueness of the plume community with distance from the source, suggesting that mixing and entrainment between downstream biotopes is negligible.

The neutrally buoyant plume is likely too chemically enriched for non-adapted microbial taxa to thrive, and consequently are outcompeted by groups that can benefit from or tolerate the chemical nature of the plume. Therefore, it is likely that less specialised groups die out due to lack of appropriate resources and interspecies competition, as indicated by the decline in biodiversity with age of plume (distance) directly mirroring the increasing dominance of Epsilonproteobacteria, a group already known to influence community structures (Opatkiewicz et al., 2009). In addition, the decrease in concentration of particulate matter may influence microbial diversity (Huber et al., 2003). Temporal succession has been observed within plume environments by Sylvan et al., 2012 and Reed et al., 2015, driven by metabolic energy yield and concentration of the electron donors. We propose that the patterns in our study reflect ecological succession (Connell and Slaytor, 1977) within the plume with change in microbial communities resulting in a low diversity, climax plume community. At the distant stations 47 and 49, the community was less dominated by Epsilonproteobacteria and more diverse, indicating a gradual return to what is likely a non-plume influenced state of the microbial community. The wide range of correlations within and between microbial classes and water properties, i.e. ranging from chemical to physical variables (Fig. S4), indicates a complex array of community drivers within the plume.

In contrast to our results, Sheik et al. (2015) and Djurhuus et al. (2017), observed decreasing Epsilonproteobacteria abundance within hundreds of metres from the source in the rising, buoyant portion of plumes generated by Indian Ocean and South Pacific vents. Interestingly, in our results Epsilonproteobacteria were least dominant in the freshest neutrally buoyant fluid at the station closest to the Rainbow vent site. It is likely that entrainment of other microbial groups within the rising portion of the plume dilutes the contribution by this group. However, Huber et al., 2003 suggested that Epsilonproteobacteria, thrive in weaker diffuse flow due to lower temperature and great electron acceptor availability. A sampling design to follow the continuity of the plume from the buoyant to the neutrally buoyant portion would be a suitable approach to fully trace the evolution of the plume from the orifice to

https://doi.org/10.5194/bg-2019-189
Preprint. Discussion started: 20 June 2019

full dilution. However, the term full dilution is ambiguous as it is unknown exactly how far the plume influences the water properties and how far the plume associated bacteria will follow, adding water column microbial community heterogeneity beyond our study spatial extent.

4.5 Possible effects of SMS mining plumes

Mining of SMS deposits will create additional plumes generated by activities of mining vehicles (resuspension) and by the discharge of solids from the surface vessel (discharge plume). It is yet unknown how these plumes will affect the ecosystem at active and inactive hydrothermal vent sites. Our study showed the influence of a natural hydrothermal plume on its environment up to 25 km away from its source and it was shown how a natural plume has a strong impact on the pelagic microbial and chemical composition, suggesting that mining plumes may cause similar changes to the background T0 state.

Excavation of SMS will cause removal of habitat by substrate extraction and resuspension of surface sediments. While large particles in the resulting plume are expected to stay close to the seafloor and eventually settle, smothering fauna in the immediate surroundings (Jones et al., 2018), smaller particles will disperse further, potentially invoking effects on a larger spatial scale. Another main concern is the discharge of mining waste, consisting of very fine unconsolidated particles, toxic metals and metal compounds (Weaver et al., 2018). Modelling the behaviour of the discharge plume generated by the proposed Solwara 1 SMS mining has shown that these plumes can extend up to 10 km from the mining site, resulting in a deposit thickness of up to 50 cm within 1 km of the discharge site (Gwyther et al., 2008; Boschen et al., 2013), smothering benthic fauna (Boschen et al., 2013; Weaver et al., 2018; Jones et al., 2018). Besides the impact caused by settling of particles from the excavation and discharge plumes, there is also the possible input of nutrients and toxins to otherwise nutrient- and toxin-poor systems, for example from oxidation of newly exposed sulfides and the subsequent release of heavy metals in the water column (Jones et al., 2018; Weaver et al., 2018).

The extent of the local impact of deep sea mining will depend on the location where the mining takes place. At an active site like the Rainbow hydrothermal vent field, we showed that even in the distant

https://doi.org/10.5194/bg-2019-189
Preprint. Discussion started: 20 June 2019

plume (25 km away from Rainbow) hydrothermal plume microbiota dominate. When a mining discharge plume at an active hydrothermal vent field would be merged with the natural plume, the local effects might be minimal since microbial communities are already adapted to the metal-rich environments (Gwyther et al., 2008). However, a mining plume consisting of a dense suspension of bottom sediment and fine-grained metal sulfides is expected to support an altered microbial community in terms of abundance and composition, impacting the hydrothermal plume community. Moreover, the effects over larger spatial scales could be multiplied because of the increased export of electron donors by mining activities. Reed et al. (2015), who studied a hydrothermal plume in the Lau basin, have shown that the export of the chemolithoautotrophs from a plume increases with increasing availability of electron donors. Dispersion of chemolithoautotrophs is variable between groups depending on the energetics of their metabolisms, for example, methanotrophs which could disperse more than 50 km, are likely to disperse further than sulfur oxidisers (Reed et al., 2015). Increased export of microbial biomass from plumes may have impact on other marine systems which are hospitable to chemolithotrophs, such as oxygen minimum zones (Dick et al., 2013) and to higher trophic levels (Phillips, 2017). At inactive sites the effect on the background fauna is also potentially large since these are not adapted to the heavy metal rich environments and the discharge plume could prove to be toxic to the fauna (Boschen et al., 2013), possibly affecting organisms at all levels of the food chain (Weaver et al., 2018). In addition, in case of multiple plumes at different depths due to stratification and vertical migration due to tidal regimes, the impacts may not be confined to a single depth band and may affect a large part of the water column, including other habitats, such as benthic habitats.

5 Conclusion

Our results demonstrate geochemically enriched plumes provide a dynamic habitat that is conducive to ecological changes in a short time span. Combining microbial and chemical analysis has proven to be a sensitive tool which enabled us to trace the hydrothermal plume beyond 25 km downstream from the vent source and also upstream of the Rainbow vent site, implying that the influence of the hydrothermal vent on the surrounding environment may reach further than previously thought. The neutrally buoyant plume

https://doi.org/10.5194/bg-2019-189
Preprint. Discussion started: 20 June 2019

580 was chemically enriched which spawned a distinct microbial biotope which was dominated by vent
581 associated species. As the plume aged and dispersed we observed alteration of the chemical composition
582 and microbial community composition of the plume, showcasing a horizontal heterogeneous plume.
583 Overall we have shown that a hydrothermal plume acts as a unique chemically enriched environment
584 where distinct and variable habitats are present.

585

586 **Author contribution**

587 GD, HDS, and FM conceptualised the study and undertook data collection. SH and DP undertook sample
588 processing and analysis with contributions from and under the supervision of FM, GD, GJR, HDS, JvB
589 and HW. SH and DP wrote the manuscript with contributions from all co-authors.

590

591 **Competing interests**

592 The authors declare that they have no conflict of interest.

593

594 **Acknowledgements**

595 This study was carried out in the framework of the TREASURE (Towards Responsible ExtrAction of
596 SUbmarine REsources) project, funded (grant number 13273) by the Applied and Engineering Sciences
597 (AES) domain of the Netherlands Organisation for Scientific Research (NWO) and by partners from the
598 Dutch maritime industry. Topsector Water, a collaborative effort of Dutch industry, academia and
599 government, funded ship time. We thank Evaline van Weerlee for assistance in DNA extraction and
600 Patrick Laan for assistance in the chemical analysis of the collected samples. We also thank the crew and
601 captain of the RV *Pelagia*, as well as NIOZ technicians for their essential assistance during cruise
602 64PE398. SH received funding from the Blue Nodules project, EC grant agreement. 688785. DP is
603 supported by the Natural Environmental Research Council [grant number NE/N012070/1]. HdS received

604 funding from TREASURE. FM is supported financially by the Innovational Research Incentives Scheme
605 of the Netherlands Organisation for Scientific Research (NWO-VIDI grant 016.161.360).

606

607 **References**

608 Agogue, H., Lamy, D., Neal, P. R., Sogin, M. L., and Herndl, G. J.: Water mass-specificity of bacterial communities
609 in the North Atlantic revealed by massively parallel sequencing, Mol Ecol, 20, 258-274, 10.1111/j.1365-
610 294X.2010.04932.x, 2011.

611 Anantharaman, K., Breier, J. A., and Dick, G. J.: Metagenomic resolution of microbial functions in deep-sea
612 hydrothermal plumes across the Eastern Lau Spreading Center, Isme J, 10, 225-239, 10.1038/ismej.2015.81, 2016.

613 Boschen, R. E., Rowden, A. A., Clark, M. R., and Gardner, J. P. A.: Mining of deep-sea seafloor massive sulfides:
614 A review of the deposits, their benthic communities, impacts from mining, regulatory frameworks and management
615 strategies, Ocean Coast Manage, 84, 54-67, https://doi.org/10.1016/j.ocecoaman.2013.07.005, 2013.

616 Caetano, M., Vale, C., Anes, B., Raimundo, J., Drago, T., Schimdt, S., Nogueira, M., Oliveira, A., and Prego, R.:
617 The Condor seamount at Mid-Atlantic Ridge as a supplementary source of trace and rare earth elements to the
618 sediments, Deep-Sea Res Pt Ii, 98, 24-37, https://doi.org/10.1016/j.dsr2.2013.01.009, 2013.

619 Cave, R. R., German, C. R., Thomson, J., and Nesbitt, R. W.: Fluxes to sediments underlying the Rainbow
620 hydrothermal plume at 36 degrees 14 ' N on the Mid-Atlantic Ridge, Geochim Cosmochim Ac, 66, 1905-1923,
621 https://doi.org/10.1016/S0016-7037(02)00823-2, 2002.

622 Cerqueira, T., Barroso, C., Froufe, H., Egas, C., and Bettencourt, R.: Metagenomic Signatures of Microbial
623 Communities in Deep-Sea Hydrothermal Sediments of Azores Vent Fields, Microb Ecol, 76, 387-403,
624 https://doi.org/10.1007/s00248-018-1144-x, 2018.

625 Charlou, J. L., Donval, J. P., Fouquet, Y., Jean-Baptiste, P., and Holm, N.: Geochemistry of high H(2) and CH(4)
626 vent fluids issuing from ultramafic rocks at the Rainbow hydrothermal field (36 degrees 14 ' N, MAR), Chem Geol,
627 191, 345-359, 2002.

628 Chavagnac, V., German, C. R., Milton, J. A., and Palmer, M. R.: Sources of REE in sediment cores from the
629 Rainbow vent site (36 degrees 14 ' N, MAR), Chem Geol, 216, 329-352, https://doi.org/10.1016/S0009-
630 2541(02)00134-1, 2005.

631 Collins, P. C., Croot, P., Carlsson, J., Colaço, A., Grehan, A., Hyeong, K., Kennedy, R., Mohn, C., Smith, S., and
632 Yamamoto, H.: A primer for the Environmental Impact Assessment of mining at seafloor massive sulfide deposits,
633 Mar Policy, 42, 198-209, https://doi.org/10.1016/j.marpol.2013.01.020, 2013.

634 Connell, J. H., and Slatyer, R. O.: Mechanisms of Succession in Natural Communities and Their Role in
635 Community Stability and Organization, Am Nat, 111, 1119-1144, https://doi.org/10.1086/283241, 1977.

636 Cowen, J. P., and Bruland, K. W.: Metal Deposits Associated with Bacteria - Implications for Fe and Mn Marine
637 Biogeochemistry, Deep-Sea Res, 32, 253-&, https://doi.org/10.1016/0198-0149(85)90078-0, 1985.

638 Cowen, J. P., Massoth, G. J., and Feely, R. A.: Scavenging Rates of Dissolved Manganese in a Hydrothermal Vent
639 Plume, Deep-Sea Res, 37, 1619-1637, https://doi.org/10.1016/0198-0149(90)90065-4, 1990.

640 Dell'Anno, A., and Corinaldesi, C.: Degradation and turnover of extracellular DNA in marine sediments: Ecological
641 and methodological considerations, Appl Environ Microb, 70, 4384-4386, 10.1128/AEM.70.7.4384–4386.2004,
642 2004.

643 Dick, G. J., Clement, B. G., Webb, S. M., Fodrie, F. J., Bargar, J. R., and Tebo, B. M.: Enzymatic microbial Mn(II)
644 oxidation and Mn biooxide production in the Guaymas Basin deep-sea hydrothermal plume, Geochim Cosmochim
645 Ac, 73, 6517-6530, https://doi.org/10.1016/j.gca.2009.07.039, 2009.

646 Dick, G. J., and Tebo, B. M.: Microbial diversity and biogeochemistry of the Guaymas Basin deep-sea
647 hydrothermal plume, Environ Microbiol, 12, 1334-1347, https://doi.org/10.1111/j.1462-2920.2010.02177.x, 2010.

648 Dick, G. J., Anantharaman, K., Baker, B. J., Li, M., Reed, D. C., and Sheik, C. S.: The microbiology of deep-sea
649 hydrothermal vent plumes: ecological and biogeographic linkages to seafloor and water column habitats, Front
650 Microbiol, 4, https://doi.org/10.3389/fmicb.2013.00124, 2013.

651 Djurhuus, A., Mikalsen, S. O., Giebel, H. A., and Rogers, A. D.: Cutting through the smoke: the diversity of
652 microorganisms in deep-sea hydrothermal plumes, Royal Society Open Science, 4,
653 https://doi.org/10.1098/rsos.160829, 2017.

654 Douville, E., Charlou, J. L., Oelkers, E. H., Bienvenu, P., Colon, C. F. J., Donval, J. P., Fouquet, Y., Prieur, D.,
655 and Appriou, P.: The rainbow vent fluids (36 degrees 14 ' N, MAR): the influence of ultramafic rocks and phase
656 separation on trace metal content in Mid-Atlantic Ridge hydrothermal fluids, Chem Geol, 184, 37-48,
657 https://doi.org/10.1016/S0009-2541(01)00351-5, 2002.

658 Dymond, J., and Roth, S.: Plume Dispersed Hydrothermal Particles - a Time-Series Record of Settling Flux from
659 the Endeavor Ridge Using Moored Sensors, Geochim Cosmochim Ac, 52, 2525-2536, 1988.

660 Edmonds, H. N., and German, C. R.: Particle geochemistry in the Rainbow hydrothermal plume, Mid-Atlantic
661 Ridge, Geochim Cosmochim Ac, 68, 759-772, 10.1016/0016-7037(88)90310-9, 2004.

662 Emery, W. J., and Meincke, J.: Global Water Masses - Summary and Review, Oceanol Acta, 9, 383-391, 1986.

663 Findlay, A. J., Gartman, A., Shaw, T. J., and Luther, G. W.: Trace metal concentration and partitioning in the first
664 1.5 m of hydrothermal vent plumes along the Mid-Atlantic Ridge: TAG, Snakepit, and Rainbow, Chem Geol, 412,
665 117-131, https://doi.org/10.1016/j.chemgeo.2015.07.021, 2015.

666 Fouquet, Y., Barriga, F., Charlou, J. L., Elderfield, H., German, C. R., Ondréas, H., Parson, L., Radford-Knoery,
667 J., Relvas, J., Ribeiro, A., Schultz, A., Apprioual, R., Cambon, P., Costa, I., Donval, J. P., Douville, E., Landuré,
668 J. Y., Normund, A., Pellé, H., Ponsevera, E., Riches, S., Santana, H., and Stephan, M.: Flores diving cruise with
669 the Nautile near the Azores. First dives on the Rainbow field: hydrothermal seawater/mantle interaction, InterRidge
670 News, 7, 24-28, 1998.

671 Frank, K. L., Rogers, D. R., Olins, H. C., Vidoudez, C., and Girguis, P. R.: Characterizing the distribution and rates
672 of microbial sulfate reduction at Middle Valley hydrothermal vents, Isme J, 7, 1391-1401,
673 https://doi.org/10.1038/ismej.2013.17, 2013.

674 German, C. R., Campbell, A. C., and Edmond, J. M.: Hydrothermal Scavenging at the Mid-Atlantic Ridge -
675 Modification of Trace-Element Dissolved Fluxes, Earth and Planetary Science Letters, 107, 101-114,
676 https://doi.org/10.1016/0012-821X(91)90047-L, 1991.

677 German, C. R., and Sparks, R. S. J.: Particle Recycling in the Tag Hydrothermal Plume, Earth and Planetary Science
678 Letters, 116, 129-134, https://doi.org/10.1016/0012-821X(93)90049-F, 1993.

679 German, C. R., Klinkhammer, G. P., and Rudnicki, M. D.: The Rainbow hydrothermal plume, 36 degrees 15'N,
680 MAR, Geophys Res Lett, 23, 2979-2982, https://doi.org/10.1029/96GL02883, 1996.

681 German, C. R., Richards, K. J., Rudnicki, M. D., Lam, M. M., Charlou, J. L., and Party, F. S.: Topographic control
682 of a dispersing hydrothermal plume, Earth and Planetary Science Letters, 156, 267-273,
683 https://doi.org/10.1016/S0012-821X(98)00020-X, 1998.

684 Gwyther, D., and Wright, M.: Environmental Impact Statement: Solwara 1, Coffey Natural Systems Pty Ltd, 47-
685 65, 2008.

686 Han, Y. C., Gonnella, G., Adam, N., Schippers, A., Burkhardt, L., Kurtz, S., Schwarz-Schampera, U., Franke, H.,
687 and Perner, M.: Hydrothermal chimneys host habitat-specific microbial communities: analogues for studying the
688 possible impact of mining seafloor massive sulfide deposits, Sci Rep-Uk, 8, 10.1038/s41598-018-28613-5, 2018.

689 Huber, J. A., Butterfield, D. A. and Baross, J. A.: Bacterial diversity in a subseafloor habitat following a deep-sea
690 volcanic eruption. FEMS Microbiol Ecol, 43(3), pp.393-409, https://doi.org/10.1111/j.1574-6941.2003.tb01080.x,
691 2003.

692 Hoagland, P., Beaulieu, S., Tivey, M. A., Eggert, R. G., German, C., Glowka, L., and Lin, J.: Deep-sea mining of
693 seafloor massive sulfides, Mar Policy, 34, 728-732, https://doi.org/10.1016/j.marpol.2009.12.001, 2010.

694 Jannasch, H. W., and Mottl, M. J.: Geomicrobiology of Deep-Sea Hydrothermal Vents, Science, 229, 717-725,
695 10.1126/science.229.4715.717, 1985.

696 Jones, D. O. B., Amon, D. L., and Chapman, A. S. A.: Mining Deep-Ocean Mineral Deposits: What are the
697 Ecological Risks?, Elements, 14, 325-330, https://doi.org/10.2138/gselements.14.5.325, 2018.

698 Juniper, S. K., Bird, D. F., Summit, M., Vong, M. P., and Baker, E. T.: Bacterial and viral abundances in
699 hydrothermal event plumes over northern Gorda Ridge, Deep-Sea Res Pt Ii, 45, 2739-2749,
700 https://doi.org/10.1016/S0967-0645(98)00091-5, 1998.

701 Khripounoff, A., Vangriesheim, A., Crassous, P., Segonzac, M., Colaco, A., Desbruyeres, D., and Barthelemy, R.:
702 Particle flux in the Rainbow hydrothermal vent field (Mid-Atlantic Ridge): Dynamics, mineral and biological
703 composition, J Mar Res, 59, 633-656, https://doi.org/10.1357/002224001762842217, 2001.

704 Lopez-Garcia, P., Philippe, H., Gail, F., and Moreira, D.: Autochthonous eukaryotic diversity in hydrothermal
705 sediment and experimental microcolonizers at the Mid-Atlantic Ridge, P Natl Acad Sci USA, 100, 697-702,
706 https://doi.org/10.1073/pnas.0235779100, 2003.

Ludford, E. M., Palmer, M. R., German, C. R., and Klinkhammer, G. P.: The geochemistry of Atlantic hydrothermal particles, Geophys Res Lett, 23, 3503-3506, https://doi.org/10.1029/96GL02078, 1996.

Mandernack, K. W., and Tebo, B. M.: Manganese Scavenging and Oxidation at Hydrothermal Vents and in Vent Plumes, Geochim Cosmochim Ac, 57, 3907-3923, 1993.

McCollom, T. M.: Geochemical constraints on primary productivity in submarine hydrothermal vent plumes, Deep-Sea Res Pt I, 47, 85-101, https://doi.org/10.1016/S0967-0637(99)00048-5, 2000.

Nakagawa, S., Takai, K., Inagaki, F., Hirayama, H., Nunoura, T., Horikoshi, K., and Sako, Y.: Distribution, phylogenetic diversity and physiological characteristics of epsilon-Proteobacteria in a deep-sea hydrothermal field, Environ Microbiol, 7, 1619-1632, https://doi.org/10.1111/j.1462-2920.2005.00856.x, 2005.

Olins, H. C., Rogers, D. R., Preston, C., Ussler, W., Pargett, D., Jensen, S., Roman, B., Birch, J. M., Scholin, C. A., Haroon, M. F., and Girguis, P. R.: Co-registered Geochemistry and Metatranscriptomics Reveal Unexpected Distributions of Microbial Activity within a Hydrothermal Vent Field, Front Microbiol, 8, https://doi.org/10.3389/fmicb.2017.01042, 2017.

Opatkiewicz, A. D., Butterfield, D. A., and Baross, J. A.: Individual hydrothermal vents at Axial Seamount harbor distinct subseafloor microbial communities, Fems Microbiol Ecol, 70, 413-424, https://doi.org/10.1111/j.1574-6941.2009.00747.x, 2009.

Phillips, B. T.: Beyond the vent: New perspectives on hydrothermal plumes and pelagic biology, Deep-Sea Res Pt Ii, 137, 480-485, https://doi.org/10.1016/j.dsr2.2016.10.005, 2017.

Ramirez-Llodra, E., Tyler, P. A., Baker, M. C., Bergstad, O. A., Clark, M. R., Escobar, E., Levin, L. A., Menot, L., Rowden, A. A., Smith, C. R., and Van Dover, C. L.: Man and the Last Great Wilderness: Human Impact on the Deep Sea, Plos One, 6, https://doi.org/10.1371/journal.pone.0022588, 2011.

Reed, D. C., Breier, J. A., Jiang, H. S., Anantharaman, K., Klausmeier, C. A., Toner, B. M., Hancock, C., Speer, K., Thurnherr, A. M., and Dick, G. J.: Predicting the response of the deep-ocean microbiome to geochemical perturbations by hydrothermal vents, Isme J, 9, 1857-1869, https://doi.org/10.1038/ismej.2015.4, 2015.

Severmann, S., Johnson, C. M., Beard, B. L., German, C. R., Edmonds, H. N., Chiba, H., and Green, D. R. H.: The effect of plume processes on the Fe isotope composition of hydrothermally derived Fe in the deep ocean as inferred

733 from the Rainbow vent site, Mid-Atlantic Ridge, 36 degrees 14' N, Earth and Planetary Science Letters, 225, 63-
734 76, https://doi.org/10.1016/j.epsl.2004.06.001, 2004.

735 Sheik, C. S., Anantharaman, K., Breier, J. A., Sylvan, J. B., Edwards, K. J., and Dick, G. J.: Spatially resolved
736 sampling reveals dynamic microbial communities in rising hydrothermal plumes across a back-arc basin, Isme J,
737 9, 1434-1445, https://doi.org/10.1038/ismej.2014.228, 2015.

738 Sunamura, M., Higashi, Y., Miyako, C., Ishibashi, J., and Maruyama, A.: Two bactetia phylotypes are predominant
739 in the Suiyo Seamount hydrothermal plume, Appl Environ Microb, 70, 1190-1198, 10.1128/AEM.70.2.1190-
740 1198.2004, 2004.

741 Thurnherr, A. M., and Richards, K. J.: Hydrography and high-temperature heat flux of the Rainbow hydrothermal
742 site (36 degrees 14 ' N, Mid-Atlantic Ridge), J Geophys Res-Oceans, 106, 9411-9426,
743 https://doi.org/10.1029/2000JC900164, 2001.

744 Thurnherr, A. M., Richards, K. J., German, C. R., Lane-Serff, G. F., and Speer, K. G.: Flow and mixing in the rift
745 valley of the Mid-Atlantic Ridge, J Phys Oceanogr, 32, 1763-1778, https://doi.org/10.1175/1520-
746 0485(2002)032<1763:FAMITR>2.0.CO;2, 2002.

747 van Bleijswijk, J. D. L., Whalen, C., Duineveld, G. C. A., Lavaleye, M. S. S., Witte, H. J., and Mienis, F.: Microbial
748 assemblages on a cold-water coral mound at the SE Rockall Bank (NE Atlantic): interactions with hydrography
749 and topography, Biogeosciences, 12, 4483-4496, https://doi.org/10.5194/bg-12-4483-2015, 2015.

750 van Haren, H., Duineveld, G., and de Stigter, H.: Prefrontal bore mixing, Geophys Res Lett, 44, 9408-9415,
751 https://doi.org/10.1002/2017GL074384, 2017.

752 Vare, L. L., Baker, M. C., Howe, J. A., Levin, L. A., Neira, C., Ramirez-Llodra, E. Z., Reichelt-Brushett, A.,
753 Rowden, A. A., Shimmield, T. M., Simpson, S. L., and Soto, E. H.: Scientific Considerations for the Assessment
754 and Management of Mine Tailings Disposal in the Deep Sea, Frontiers in Marine Science, 5,
755 https://doi.org/10.3389/fmars.2018.00017, 2018.

756 Von Damm, K. L.: Evolution of the hydrothermal system at East Pacific Rise 9 50 N: geochemical evidence for
757 changes in the upper oceanic crust, Mid-Ocean Ridges: Hydrothermal Interactions Between the Lithosphere and
758 Oceans, 148, 285-304, https://doi.org/10.1029/148GM12, 2004.

https://doi.org/10.5194/bg-2019-189
Preprint. Discussion started: 20 June 2019

759 Weaver, P. P., Billett, D. S., and Van Dover, C. L.: Environmental risks of deep-sea mining, in: Handbook on
760 Marine Environment Protection, Springer, 215-245, https://doi.org/10.1007/978-3-319-60156-4_11, 2018.

761 Wetzel, L. R., and Shock, E. L.: Distinguishing ultramafic- from basalt-hosted submarine hydrothermal systems
762 by comparing calculated vent fluid compositions, J Geophys Res-Sol Ea, 105, 8319-8340,
763 https://doi.org/10.1029/1999JB900382, 2000.

764 Winn, C. D., Karl, D. M., and Massoth, G. J.: Microorganisms in Deep-Sea Hydrothermal Plumes, Nature, 320,
765 744-746, https://doi.org/10.1038/320744a0, 1986.

766 Yilmaz, P., Parfrey, L.W., Yarza, P., Gerken, J., Pruesse, E., Quast, C., Schweer, T., Peplies, J., Ludwig, W. and
767 Glöckner, F.O.: The SILVA and "all-species living tree project (LTP)" taxonomic frameworks. Nucleic Acids Res,
768 42(D1), pp.D643-D648, https://doi.org/10.1093/nar/gkt1209, 2014.

769 Zinger, L., Amaral-Zettler, L. A., Fuhrman, J. A., Horner-Devine, M. C., Huse, S. M., Welch, D. B. M., Martiny,
770 J. B. H., Sogin, M., Boetius, A., and Ramette, A.: Global Patterns of Bacterial Beta-Diversity in Seafloor and
771 Seawater Ecosystems, Plos One, 6, https://doi.org/10.1371/journal.pone.0024570, 2011.

772

773

https://doi.org/10.5194/bg-2019-189
Preprint. Discussion started: 20 June 2019

774 **Figures and tables**

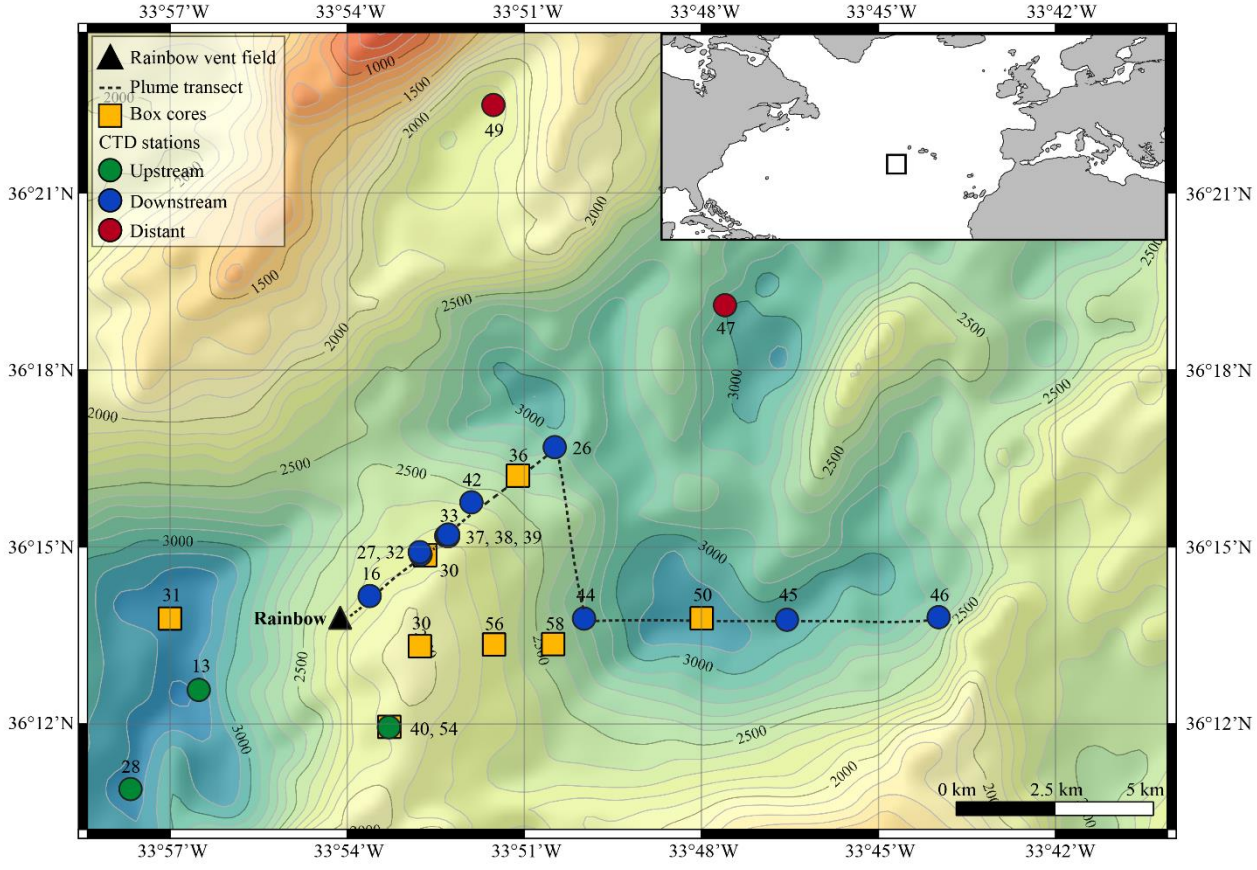

775

776 *Figure 1: Mid Atlantic Ridge bathymetry (EMOD) with Geographical location (inset), showing sampling methods*
777 *and locations depicted.*

778

https://doi.org/10.5194/bg-2019-189
Preprint. Discussion started: 20 June 2019

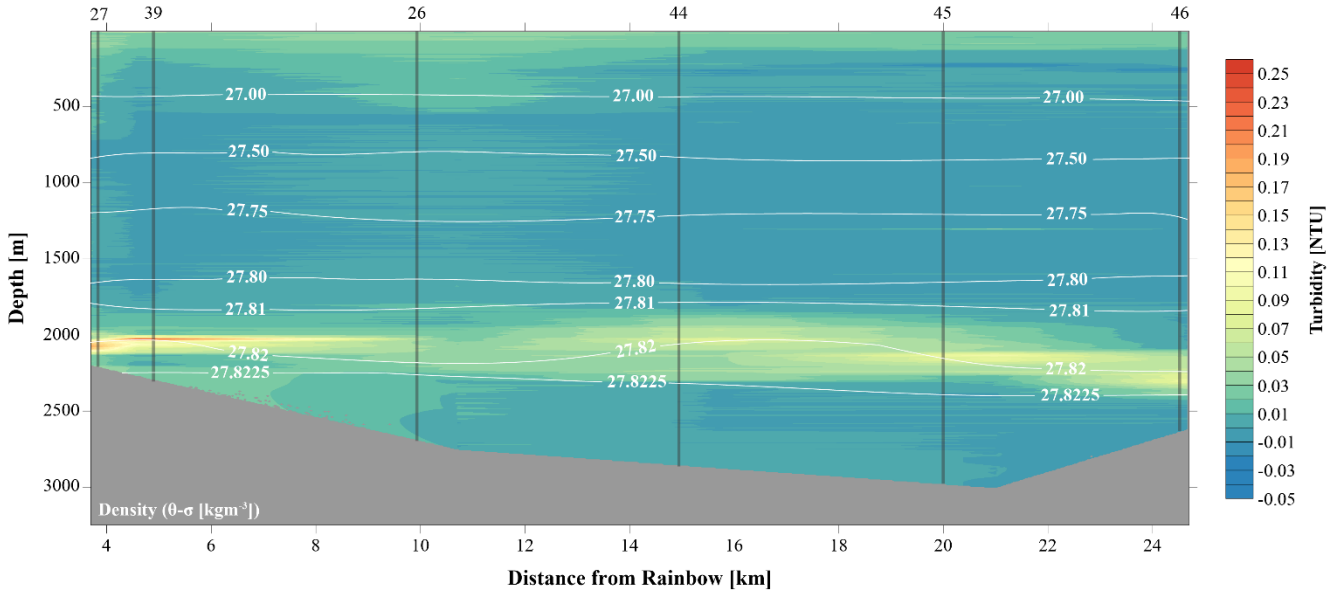

Figure 2: Transect along main plume path showing turbidity in the water column. The plume is indicated by highest turbidity values and disperses away from the Rainbow vent field.

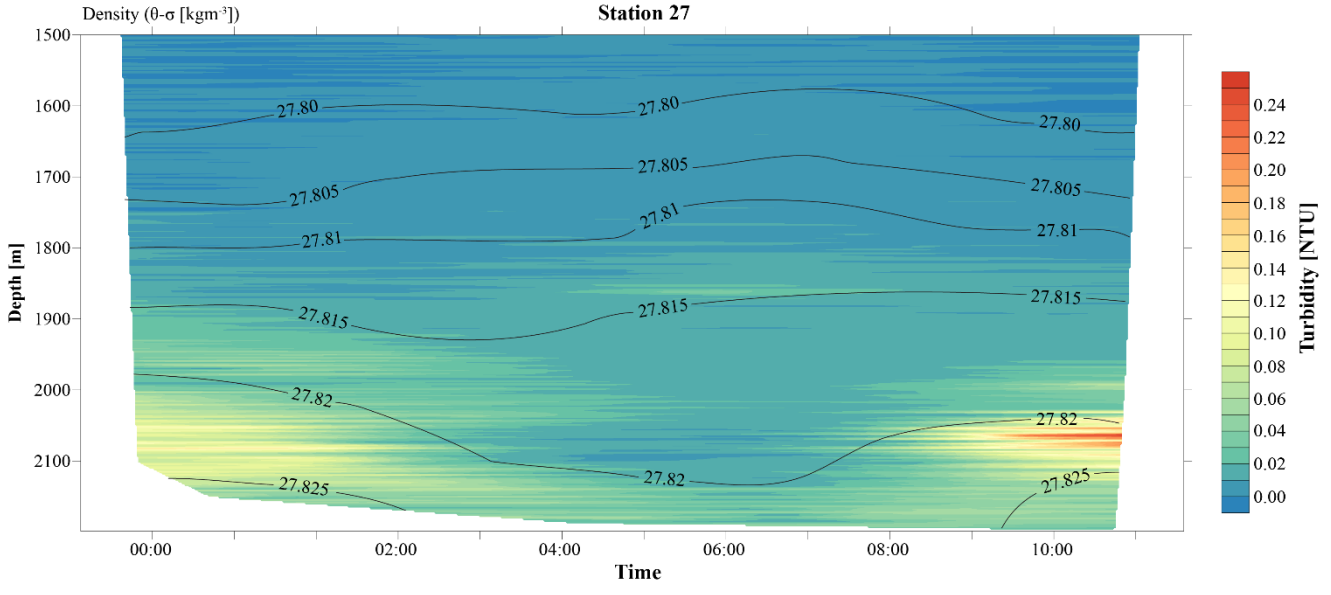

Figure 3: 12 hour CTD YOYO casts at station 27 showing the temporal evolution of the hydrothermal plume over a tidal cycle.

https://doi.org/10.5194/bg-2019-189
Preprint. Discussion started: 20 June 2019

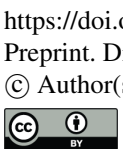

Biogeosciences
Discussions
Open Access
EGU

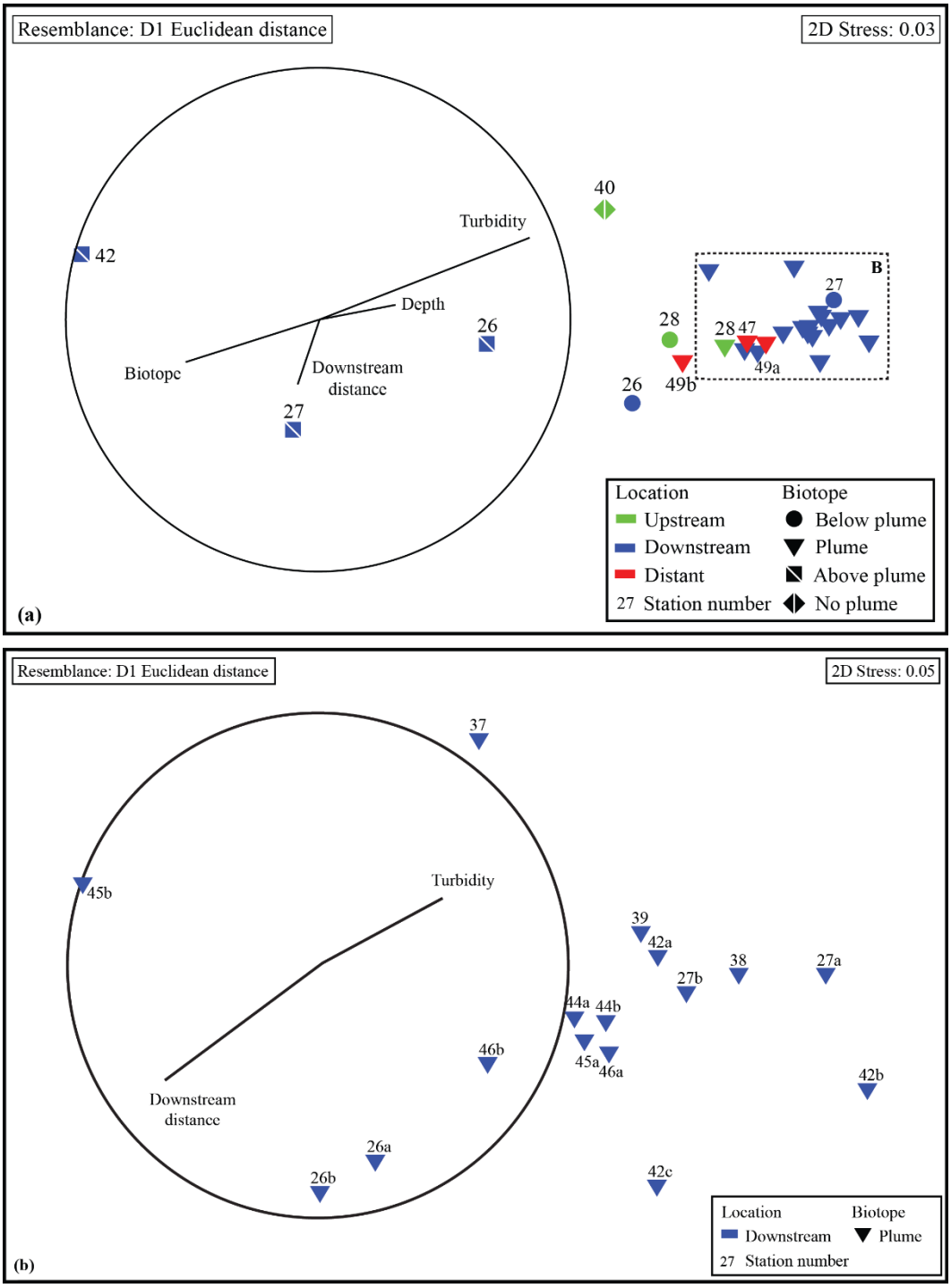

787

788 *Figure 4: (a) NMDS ordination showing all water samples based on their resemblance in chemical composition.*
789 *(b) NMDS ordination showing all plume samples from the downstream stations based on their resemblance in*
790 *chemical composition.*

https://doi.org/10.5194/bg-2019-189
Preprint. Discussion started: 20 June 2019

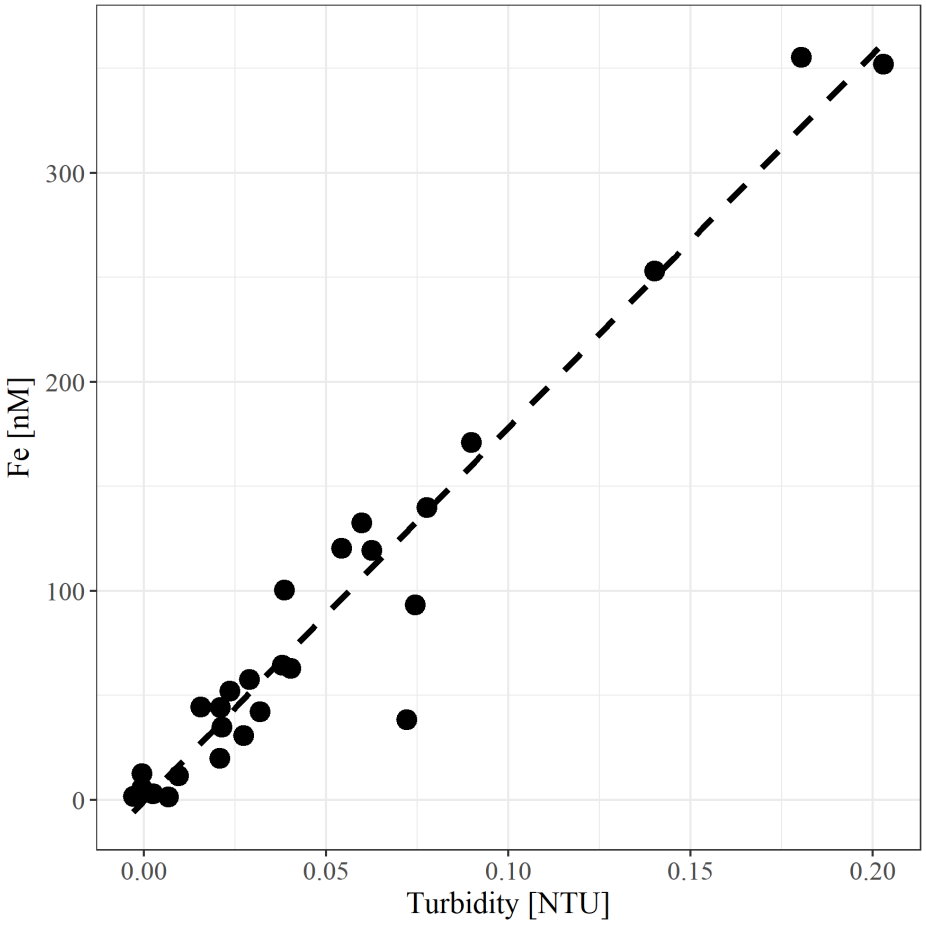

Figure 5: Relationship between measured turbidity and molar concentration of iron.

https://doi.org/10.5194/bg-2019-189
Preprint. Discussion started: 20 June 2019

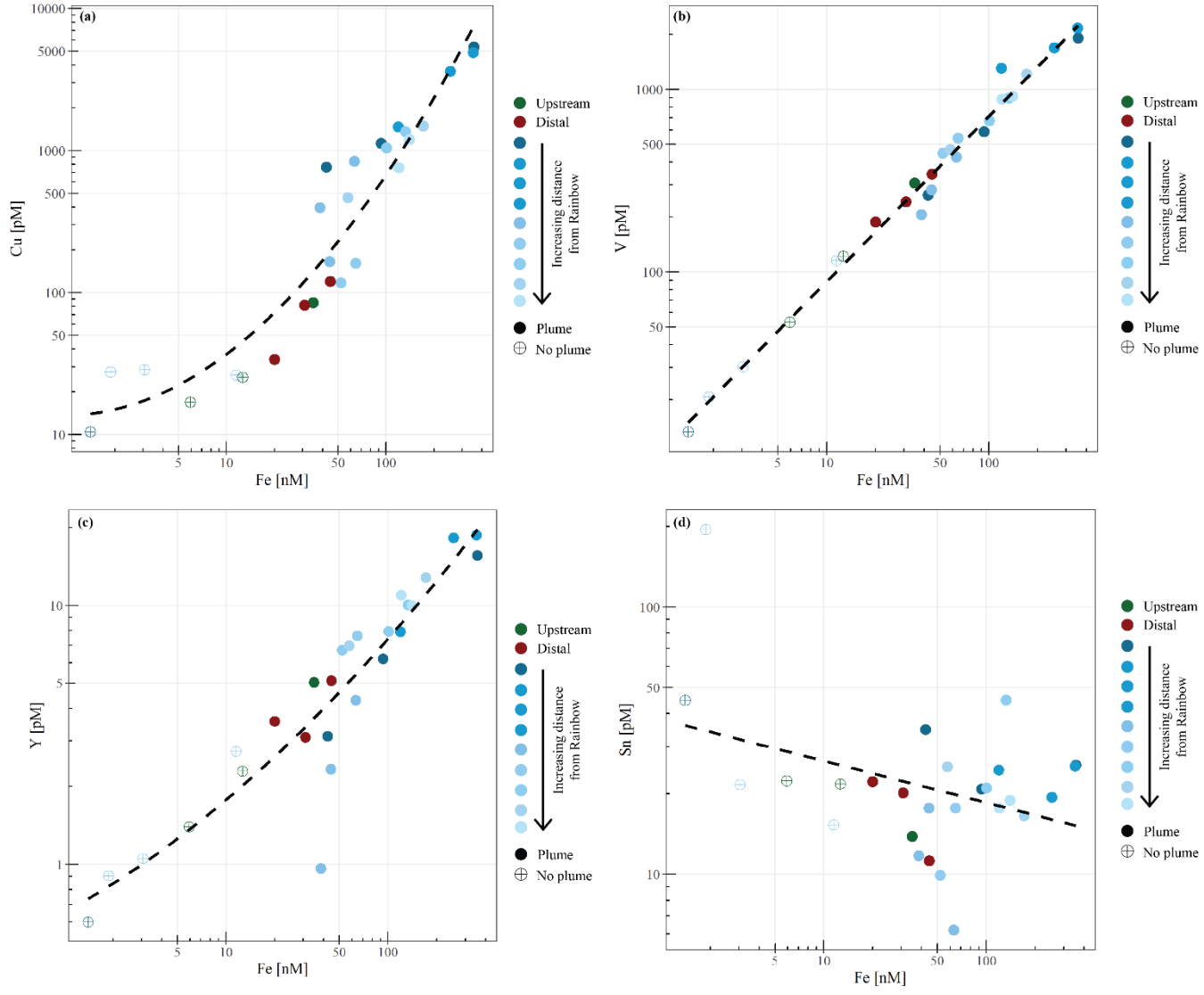

Figure 6: Relationship between copper (a), vanadium (b), yttrium (c) and tin (d) to iron.

https://doi.org/10.5194/bg-2019-189
Preprint. Discussion started: 20 June 2019

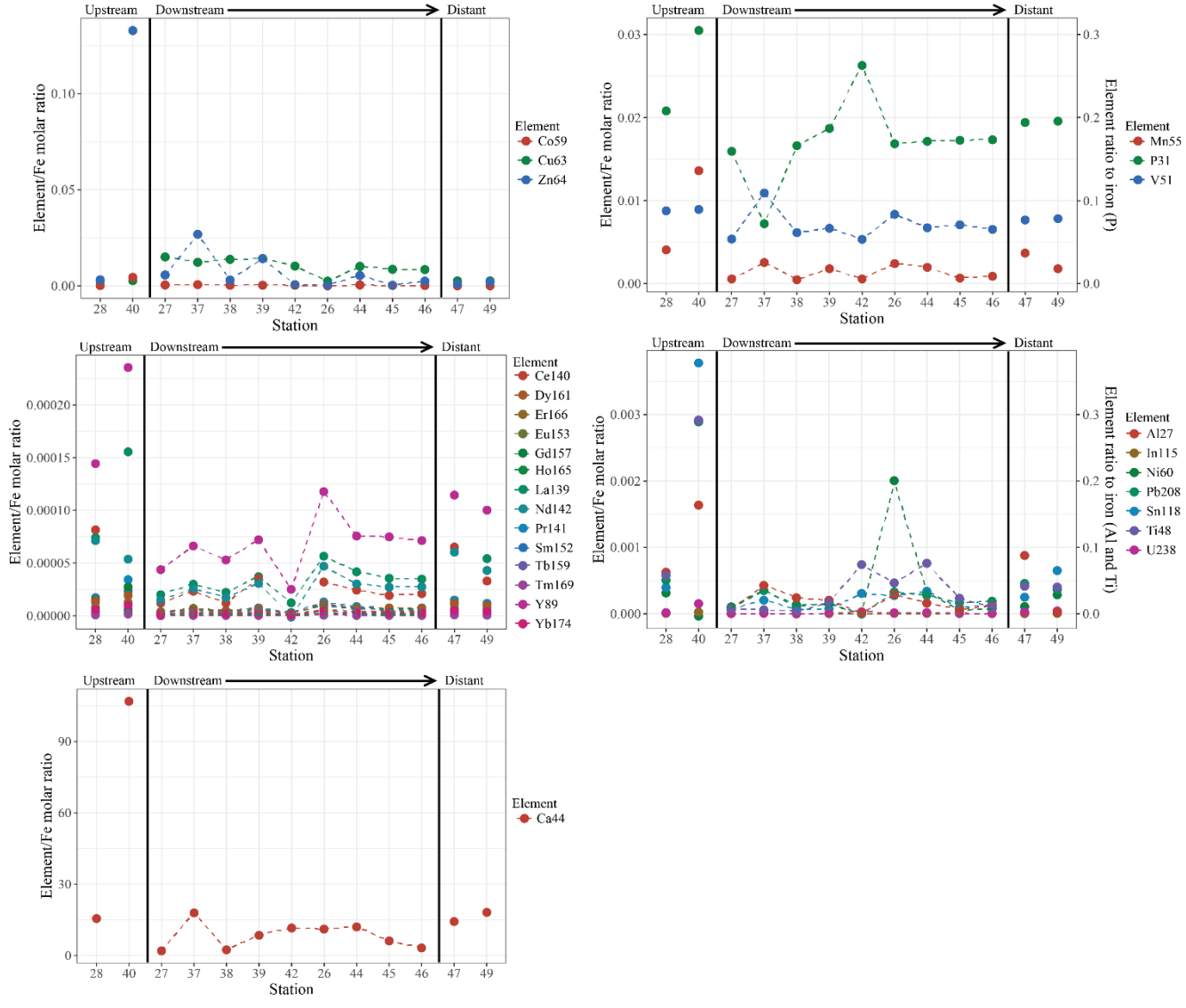

Figure 7: Element to iron molar ratios. Plume samples of upstream, downstream and distant stations. Downstream stations follow the main path of the plume. Fig. 7a) shows the element/Fe molar ratios of the chalcophiles (Co, Cu and Zn), b) shows the ratios of Mn and the oxyanions (P and V), c) displays the ratios of REE, d) the ratios of Al, In, Ni, Pb, Sn, Ti and U and e) shows the Ca/Fe molar ratio.

https://doi.org/10.5194/bg-2019-189
Preprint. Discussion started: 20 June 2019

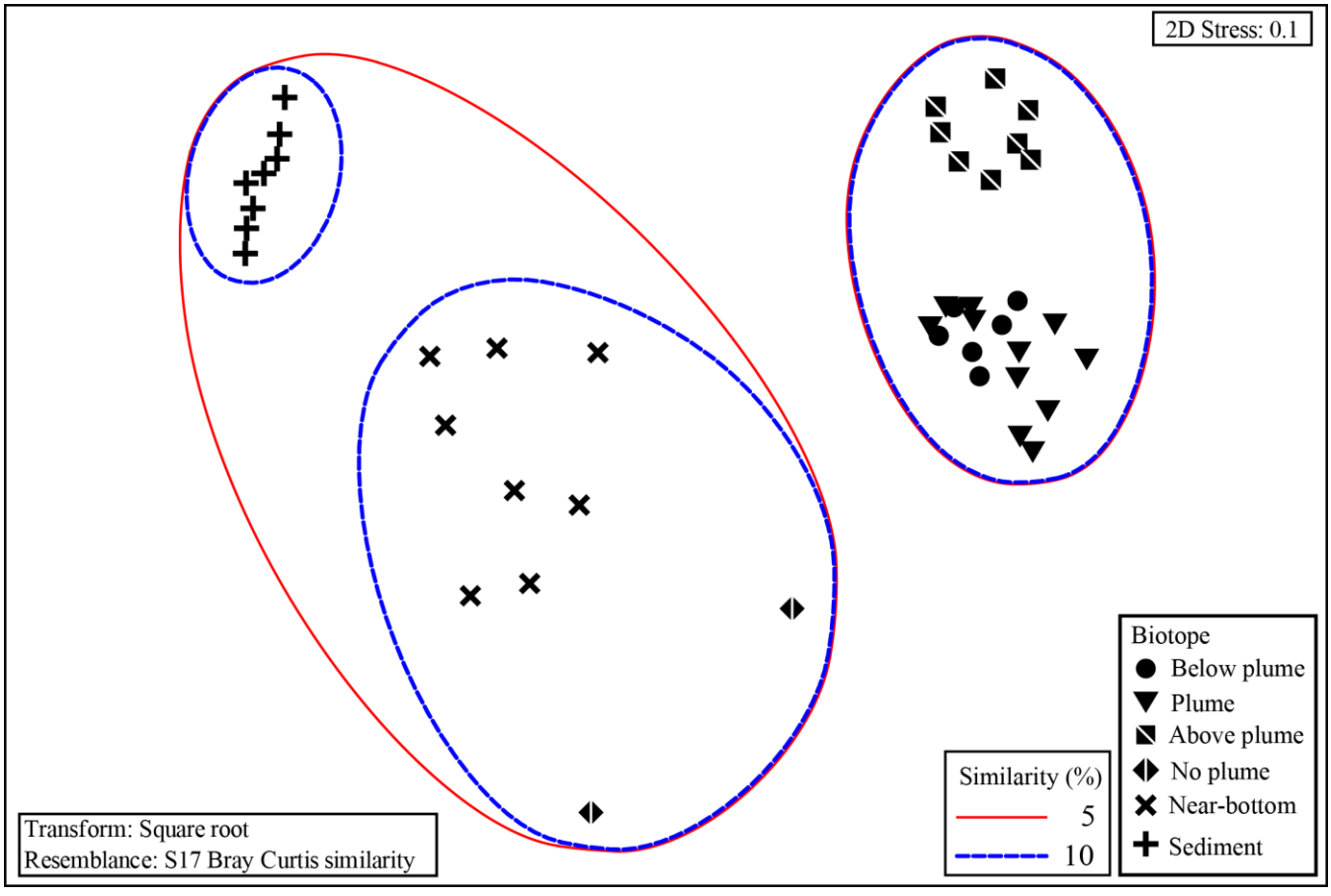

Figure 8: Non-metric multidimensional scaling plot of the microbial community composition of all samples based on Operational Taxonomic units. Similarity groupings are based on group average clustering. "No plume" is representative of samples collected from station 13, where there was no indication of a plume.

https://doi.org/10.5194/bg-2019-189
Preprint. Discussion started: 20 June 2019

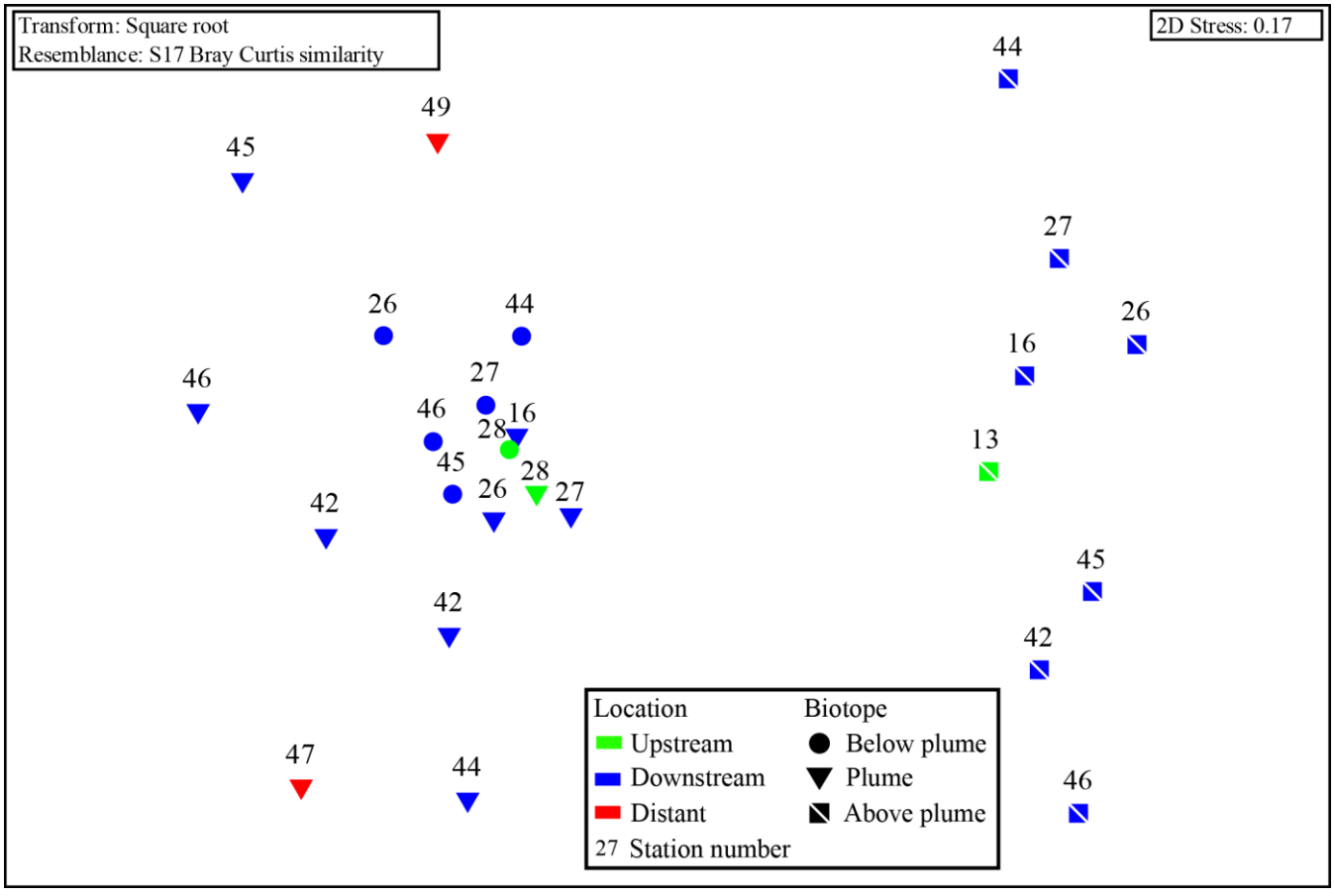

808

809 *Figure 9: Non-metric multidimensional scaling plot of the microbial community composition of all water column*
810 *samples based on Operational Taxonomic units. Plume and below plume depths from Station 13 were excluded.*

811

https://doi.org/10.5194/bg-2019-189
Preprint. Discussion started: 20 June 2019

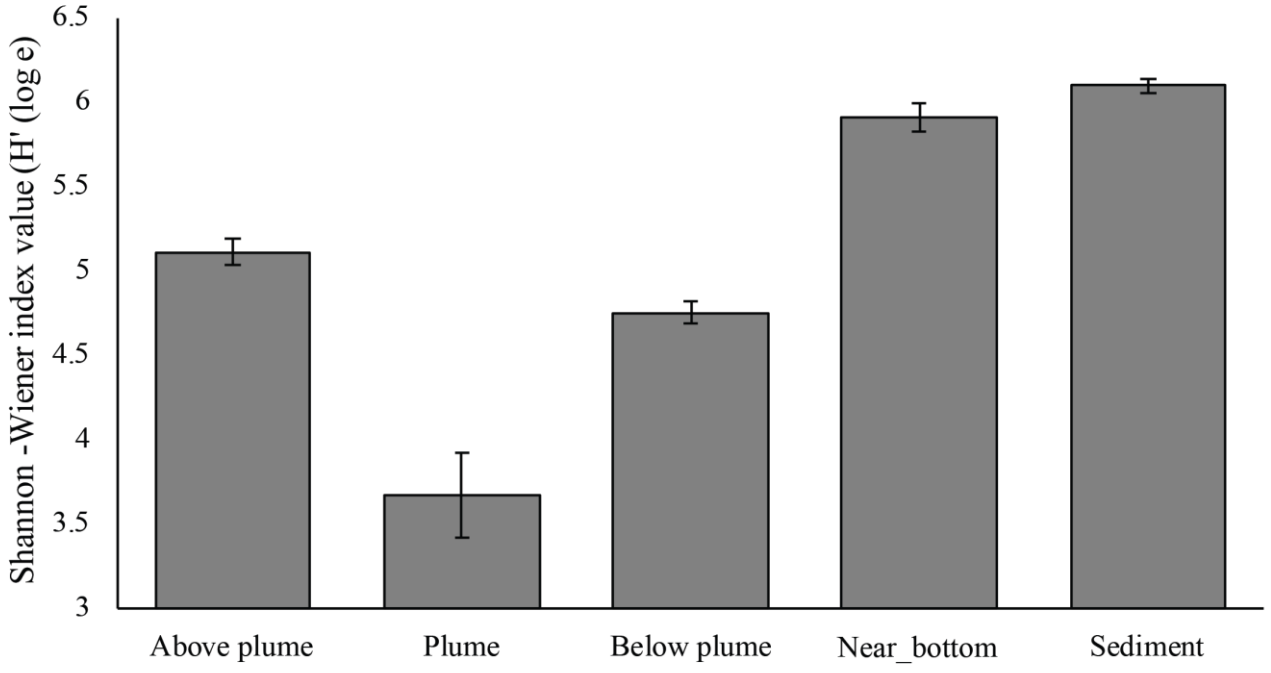

812

813 *Figure 10: Mean Shannon-Wiener diversity index for microorganisms in each biotope. Error bars represent ±SE*

814

https://doi.org/10.5194/bg-2019-189
Preprint. Discussion started: 20 June 2019

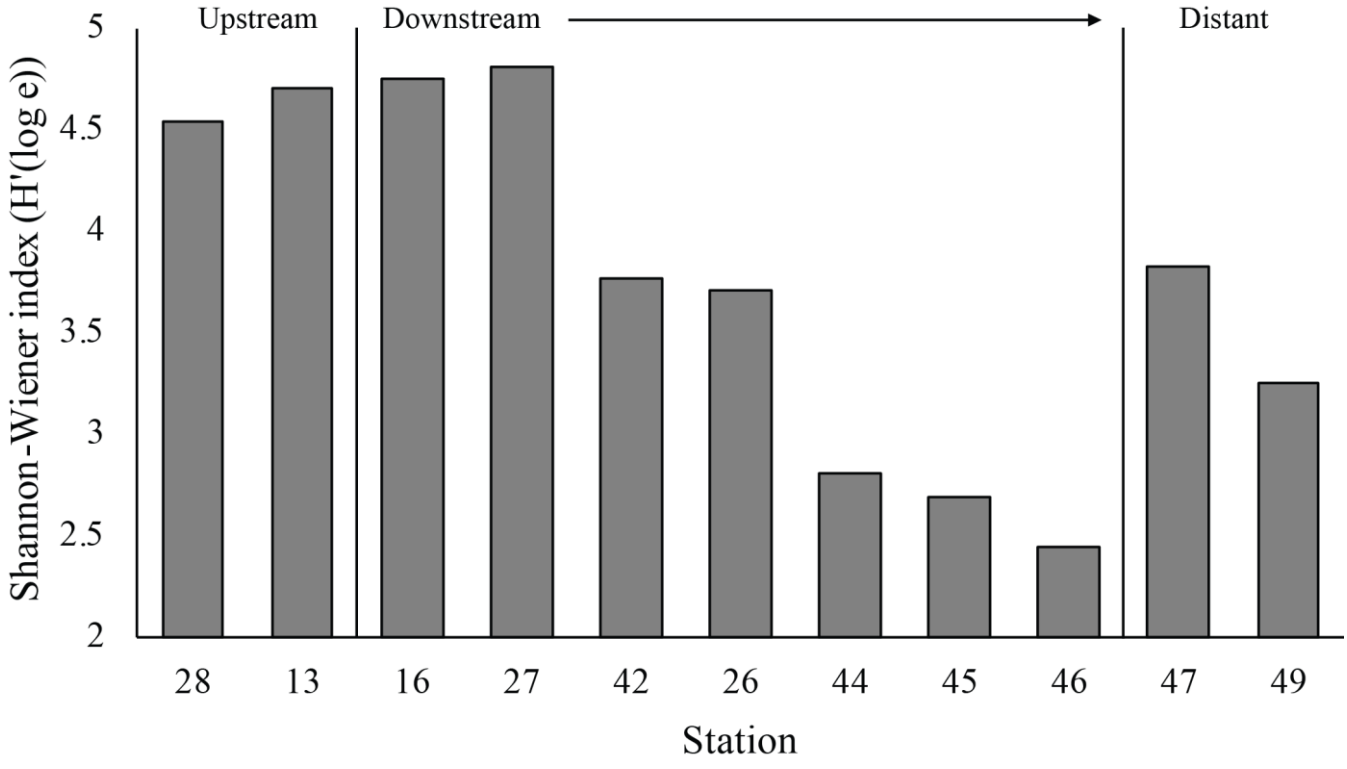

Figure 11: Shannon-Wiener index values for microorganisms in each plume sample taken.

https://doi.org/10.5194/bg-2019-189
Preprint. Discussion started: 20 June 2019

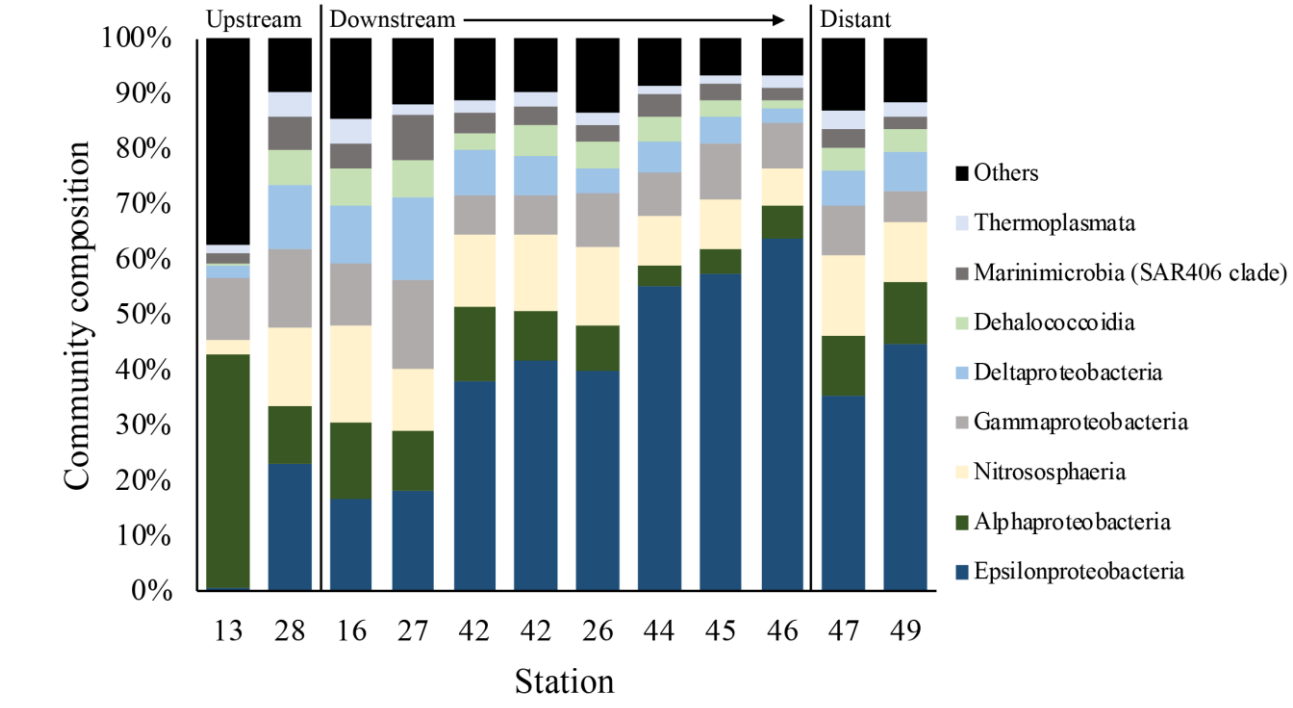

818

819 *Figure 12: Microbial community composition in the plume samples as a percentage of the dominant class groups*
820 *in accordance with the SIMPER results.*

821

https://doi.org/10.5194/bg-2019-189
Preprint. Discussion started: 20 June 2019

822 *Table 1: Meta-data of samples taken.*

Station	Biotope	Sample type	Depth(m)	C/N	Microbiology	SPM	(Trace) metals
30	Sediment and near-bottom water	Box core	1970		x		
31	Sediment and near-bottom water	Box core	3190		x		
33	Sediment and near-bottom water	Box core	2223		x		
36	Sediment and near-bottom water	Box core	2857		x		
50	Sediment and near-bottom water	Box core	3157		x		
54	Sediment and near-bottom water	Box core	2129		x		
56	Sediment and near-bottom water	Box core	2198		x		
58	Sediment and near-bottom water	Box core	2514		x		
13	Above plume	CTD	125	x	x		
13	Below plume	CTD	3220	x	x		
13	Plume	CTD	2000	x	x		
16	Plume	CTD	1944		x		
16	Above plume	CTD	998		x		
26	Below plume	CTD	2756	x	x	x	x
26a	Plume	CTD	2150	x	x	x	x
26b	Plume	CTD	2000			x	x
26	Above plume	CTD	999		x	x	x
27	Below plume	CTD	2191		x		x
27a	Plume	CTD	2077		x		x
27b	Plume	CTD	1996				x
27	Above plume	CTD	994		x		x
28	Below plume	CTD	3170	x	x	x	x
28	Plume	CTD	1975	x	x	x	x
32a	Plume	CTD	2192			x	
32b	Plume	CTD	2088			x	
37	Plume	CTD	2190				x
38	Plume	CTD	2040				x
39	Plume	CTD	2019				x
40	No plume	CTD	2120				x
42a	Plume	CTD	2291	x	x	x	x
42b	Plume	CTD	2209	x	x	x	x
42c	Plume	CTD	2037			x	x
42	Above plume	CTD	999	x	x	x	x
44	Below plume	CTD	2623	x	x		
44a	Plume	CTD	2202			x	x
44b	Plume	CTD	2002	x	x	x	x
44	Above plume	CTD	995		x		
45	Below plume	CTD	3004	x	x		
45a	Plume	CTD	2166			x	x
45b	Plume	CTD	2002	x	x	x	x
45	Above plume	CTD	996		x		
46	Below plume	CTD	2622	x	x		
46a	Plume	CTD	2280	x	x	x	x
46b	Plume	CTD	2145			x	x
46	Above plume	CTD	1000		x		
47	Below plume	CTD	2850	x			
47	Plume	CTD	2200	x	x		x
49a	Plume	CTD	2260	x	x	x	x
49b	Plume	CTD	1902			x	x

823

https://doi.org/10.5194/bg-2019-189
Preprint. Discussion started: 20 June 2019

824 *Table 2: Primers used for sequencing.*

Forward		Reverse			
Primer name	Primer sequence 5'-3'	Primer name	Primer sequence 5'-3'	Ratio in mix	Reference
Arch-0519-a-S-1 (universal)	CAGCMGCCGCGGTAA	Bact-0785-b-A-18 (universal)	TACNVGGGTATCTAATCC	3/9 + 3/9	Klindworth et al. 2012
Bact-0519F (targets WS6, TM7, OP11	CAGCAGCATCGGTVA			1/9	This paper
Nano-0519F (targets Nanoarchaea)	CAGTCGCCRCGGGAA	Nano-0785R (targets Nanoarchaea)	TACNVGGGTMTCTAATYY	1/9+1/9	This paper

825

826

https://doi.org/10.5194/bg-2019-189
Preprint. Discussion started: 20 June 2019

827 *Table 3: SIMPER similarity results of each biotope at class level. ** undefined class.*

Biotope	Average similarity (%)	Class	Average proportion (%)	Average similarity	Sim/SD	Contribution (%)	Cumulative %
Above plume	82.34	Nitrososphaeria	27.10	22.79	4.61	27.67	27.67
		Alphaproteobacteria	18.34	15.22	4.15	18.49	46.16
		Gammaproteobacteria	13.44	11.58	5.52	14.07	60.23
		Deltaproteobacteria	10.67	8.46	3.38	10.27	70.50
		Marinimicrobia (SAR406 clade)	8.22	6.96	6.07	8.46	78.96
		Dehalococcoidia	6.38	5.69	9.19	6.91	85.87
		Thermoplasmata	2.63	2.26	5.68	2.74	88.61
		Acidimicrobiia	2.13	1.89	8.62	2.30	90.91
Plume	76.74	Epsilonproteobacteria	39.59	30.29	2.53	39.47	39.47
		Nitrososphaeria	12.16	10.32	4.05	13.45	52.92
		Gammaproteobacteria	9.69	7.92	4.71	10.32	63.23
		Alphaproteobacteria	9.23	7.22	2.44	9.40	72.64
		Deltaproteobacteria	7.60	5.56	2.75	7.25	79.88
		Dehalococcoidia	4.57	3.55	2.58	4.63	84.51
		Marinimicrobia (SAR406 clade)	4.02	3.07	3.83	4.00	88.51
		Thermoplasmata	2.56	1.94	3.39	2.53	91.04
Below plume	77.94	Nitrososphaeria	22.35	16.60	3.29	21.30	21.30
		Alphaproteobacteria	13.26	11.43	5.18	14.67	35.97
		Deltaproteobacteria	10.88	9.25	8.31	11.87	47.84
		Gammaproteobacteria	10.60	8.89	7.78	11.40	59.24
		Epsilonproteobacteria	9.65	7.18	2.50	9.22	68.46
		Dehalococcoidia	7.84	6.97	7.89	8.95	77.40
		Marinimicrobia (SAR406	6.32	4.49	2.31	5.76	83.16
		Thermoplasmata	4.69	3.04	2.20	3.90	87.07
		Phycisphaerae	1.97	1.75	7.60	2.24	89.31
		Planctomycetacia	2.03	1.50	2.96	1.93	91.23
Near-bottom water	75.71	Gammaproteobacteria	20.79	16.77	3.18	22.15	22.15
		Nitrososphaeria	16.90	13.54	3.79	17.89	40.04
		Alphaproteobacteria	15.55	13.25	5.47	17.50	57.54
		Deltaproteobacteria	6.68	5.89	5.99	7.78	65.32
		Oxyphotobacteria	5.93	4.04	2.18	5.34	70.66
		Dehalococcoidia	4.08	2.99	2.50	3.95	74.61
		Phycisphaerae	3.72	2.57	2.03	3.40	78.01
		Thermoplasmata	2.47	1.70	2.25	2.24	80.25
		Acidimicrobiia	2.06	1.61	2.72	2.13	82.38
		Bacteroidia	2.15	1.57	1.85	2.07	84.45
		Marinimicrobia (SAR406 clade)	1.75	1.24	2.17	1.64	86.09
		OM190	1.64	1.14	2.02	1.51	87.60
		Planctomycetacia	1.40	1.09	2.76	1.44	89.04
		Epsilonproteobacteria	1.71	0.85	1.08	1.12	90.16
Sediment	82.51	Gammaproteobacteria	29.67	27.17	8.51	32.93	32.93
		Alphaproteobacteria	13.98	12.44	4.88	15.07	48.01
		Deltaproteobacteria	11.98	10.98	10.24	13.30	61.31
		Nitrososphaeria	7.73	5.69	3.74	6.90	68.21
		Phycisphaerae	5.46	5.01	7.85	6.07	74.28
		Dehalococcoidia	3.35	2.48	2.58	3.01	77.29
		BD2-11 terrestrial group	2.36	1.91	2.90	2.31	79.60
		Subgroup 22 (Acidobacteria)	2.10	1.74	3.22	2.11	81.71
		OM190	2.09	1.50	5.50	1.81	83.53
		Nitrospira	1.79	1.49	3.68	1.80	85.33
		Bacteroidia	1.91	1.48	3.66	1.79	87.12
		Acidimicrobiia	1.58	1.24	2.84	1.50	88.62
		Thermoanaerobaculia	1.41	1.07	3.25	1.30	89.92
		Gemmatimonadetes**	1.57	1.06	1.56	1.28	91.21

828